Seminars in
NUCLEAR
MEDICINE

Advances in Dosimetry and Imaging for ^{203}Pb and ^{212}Pb Radiotheranostics

Keamogetswe Ramonaheng,[*,†] Milani Qebetu,[*,†] Kaluzi Banda,[*,†] Pryaska Goorhoo,[*,†] Khomotso Legodi,[*] Sipho Mdanda,[*,†] Sandile Sibiya,[*,†] Yonwaba Mzizi,[*,†] Honest Ndlovu,[*,†] Joseph Kabunda,[*,†] Mengdie Yang,[‡,§] Kuangyu Shi,[§] and Mike Sathekge[*,†]

Targeted alpha therapy (TAT) with ^{212}Pb is rapidly emerging as a potent modality for cancer treatment due to the high linear energy transfer and short path length of α-particles, which enable precise tumor cell killing while sparing surrounding healthy tissue. Its elementally identical theranostic partner, ^{203}Pb, functions as a γ-emitting surrogate for quantitative SPECT imaging, providing essential information for patient-specific dosimetry and treatment planning. Advances in SPECT imaging, ranging from NaI(Tl)-based dual-head systems to CZT multi-detector gamma cameras, have enhanced spatial resolution, quantitative accuracy, and lesion detectability, enabling rapid patient scanning and improved activity quantification for dosimetry. Clinical dosimetry workflows that integrate serial ^{203}Pb SPECT/CT acquisitions, pharmacokinetic modeling, and image-based activity quantification facilitate reliable generation of time−activity curves and absorbed dose estimates. Organ-level and voxel-based dosimetry, combined with advanced reconstruction and microdosimetric modeling, further refine dose calculations, supporting individualized therapy planning. Collectively, these developments highlight the translational potential of the ^{203}Pb/^{212}Pb theranostic pair. The aim of this review is to provide a comprehensive assessment of ^{212}Pb-TAT, encompassing clinical applications, surrogate imaging with ^{203}Pb, gamma camera performance, dosimetry workflows, and predictive activity quantification, illustrating how these advances collectively enable quantitative, patient-specific, and theranostic-integrated radionuclide therapy.

Semin Nucl Med 55:1011-1031

Introduction

Targeted radionuclide therapy (TRT) has emerged as a transformative modality in cancer treatment, leveraging radiopharmaceuticals to selectively deliver cytotoxic radiation to malignant cells while minimizing exposure to surrounding healthy tissues. This precision-based approach has gathered increasing attention for its ability to achieve potent, localized therapeutic effects. TRT is undergoing rapid advancement, driven by the development of novel imaging and therapeutic radiopharmaceuticals.[1,2] These innovations are reshaping the landscape of precision oncology and hold the potential to markedly improve patient outcomes.[3-16]

Within this evolving field, targeted alpha therapy (TAT) has gained considerable global interest due to the distinct physical and biological advantages of α-particle emitters over conventional β-particle radionuclide therapies.[3,5,8,17-19] Alpha particles exhibit high linear energy transfer (LET) and a short path length, generating densely ionizing tracks that induce highly localized Deoxyribonucleic acid (DNA)

---

*Nuclear Medicine Research Infrastructure (NuMeRI) NPC, Pretoria, South Africa.

†Department of Nuclear Medicine, University of Pretoria, Steve Biko Academic Hospital, Pretoria, South Africa.

‡Department of Nuclear Medicine, Shanghai Tenth People's Hospital and Institute of Nuclear Medicine, Tongji University School of Medicine, Shanghai, China.

§Department of Nuclear Medicine, Inselspital Bern University Hospital, University of Bern, Bern, Switzerland.

Address reprint requests to Keamogetswe Ramonaheng, Nuclear Medicine Research Infrastructure (NuMeRI) NPC, NuMeRI Main Centre Steve Biko & Malan Street Capital Park, Pretoria, 0084. E-mail: kamo.ramonaheng@sanumeri.co.za

https://doi.org/10.1053/j.semnuclmed.2025.09.006

damage that is inefficiently repaired, thereby promoting enhanced radiation-induced cell death.[20,21] Auger electrons, characterized by nanometre-scale ranges, deposit energy in close proximity to DNA, producing highly localized and complex DNA damage that are often irreparable. The restricted tissue penetration of these emissions confines the absorbed radiation dose to the targeted lesion while minimizing irradiation of surrounding normal tissues[22,23] as illustrated in Figure 1.

Alpha particles exhibit an LET of ~50-230 keV/μm (with tissue penetration depth of 50-100μm), producing dense ionization tracks that induce a high frequency of irreparable double-strand DNA breaks.[24-26] This property translates into a markedly enhanced relative biological effectiveness (RBE) compared with β-emitting radionuclide therapies.[22,27-38] This pronounced cytotoxicity renders α-emitters ideally suited for eradicating small, metastatic tumors while minimizing radiation-induced toxicity to normal tissues.[22] Notably, their cytotoxic efficiency is estimated to be several hundred-fold greater than that of β-particles, emphasizing the critical need for precise delivery strategies.

Exploiting their unique radiobiological properties, α-emitters in TAT have demonstrated potent, highly localized antitumor effects and are under investigation across a wide spectrum of malignancies, including prostate, breast, ovarian, melanoma, renal, lung, and bladder cancers, as well as brain tumors, neuroendocrine tumors, and leukemia.[39]

A critical challenge unique to TAT is nuclear recoil, whereby daughter nuclei produced during α-decay acquire recoil energies exceeding 100 keV, several orders of magnitude greater than typical chemical bond energies, resulting in inevitable bond rupture.[40,41] This process can drive the redistribution of radioactive daughters, many of which are thereby introducing the risk of unintended irradiation to healthy tissues and complicating internal dosimetry and safety assessments. Strategies under investigation to mitigate these effects include encapsulation of α-emitters within nanocarriers, rapid intracellular sequestration, and local intratumoural administration.[18]

The selection of an appropriate therapeutic TAT radionuclide requires initial consideration of its physical half-life, which must align with the biological half-life of the targeting vector to ensure adequate tumor retention and effective radiation dose delivery.[42,43] Beyond the physical half-life, the emission profile of a radionuclide is critical. Radionuclides that release both penetrating photons and short-range particles provide a theranostic duality, enabling non-invasive imaging for patient-specific dosimetry while simultaneously delivering highly localized cytotoxic effects. In this regard, the exceptional therapeutic potency of α-particles is particularly advantageous. Consequently, substantial research has centered on candidate α-emitters for TAT, with Lead-212 (^{212}Pb), Bismuth-212 (^{212}Bi), Bismuth-213 (^{213}Bi), Actinium-225 (^{225}Ac), Radium-224 (^{224}Ra), Astatine-211 (^{211}At), Radium-223 (^{223}Ra) and Terbium-149 (^{149}Tb) representing the principal radionuclides under investigation.

Among the candidate α-emitters, ^{212}Pb ($T_{1/2}$ = 10.6 h), which was first introduced in clinical applications by Meredith et al.,[44,45] has emerged as particularly promising due to its favorable decay characteristics (Fig. 2). ^{212}Pb undergoes β^--decay to ^{212}Bi, which then follows 2 distinct decay branches: (1) β^--decay to Polonium-212 (^{212}Po) with subsequent prompt α-emission of 8.79 MeV, and (2) direct α-emission to Thallium-208 (^{208}Tl), releasing a 6.21 MeV α-particle.[46] Together, these branching pathways produce a clinically significant cascade of high-energy α-particles capable of inducing complex, irreparable DNA damage. In addition to its strong therapeutic effect, the 10.6 h physical half-life of ^{212}Pb provides a

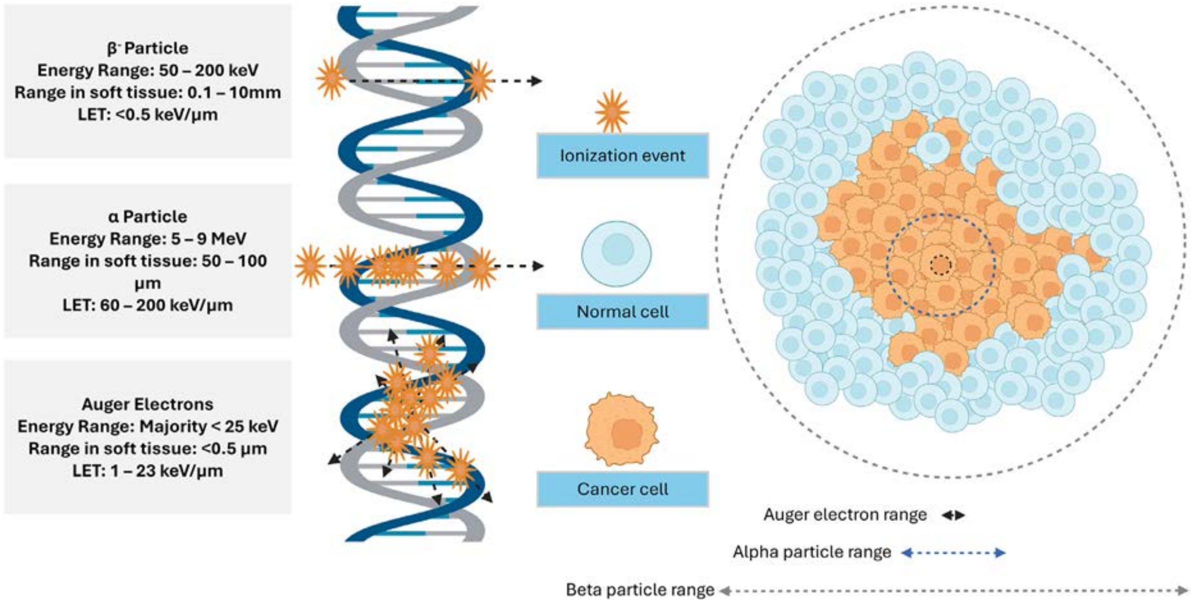

Figure 1 Targeted alpha therapy radiobiology: High-LET radiation particles induce dense track ionisations resulting in irreparable DNA damage; relative ranges of Auger electrons, α-, and β-particles (not to scale) illustrate tumour targeting with minimal healthy tissue exposure.[23]

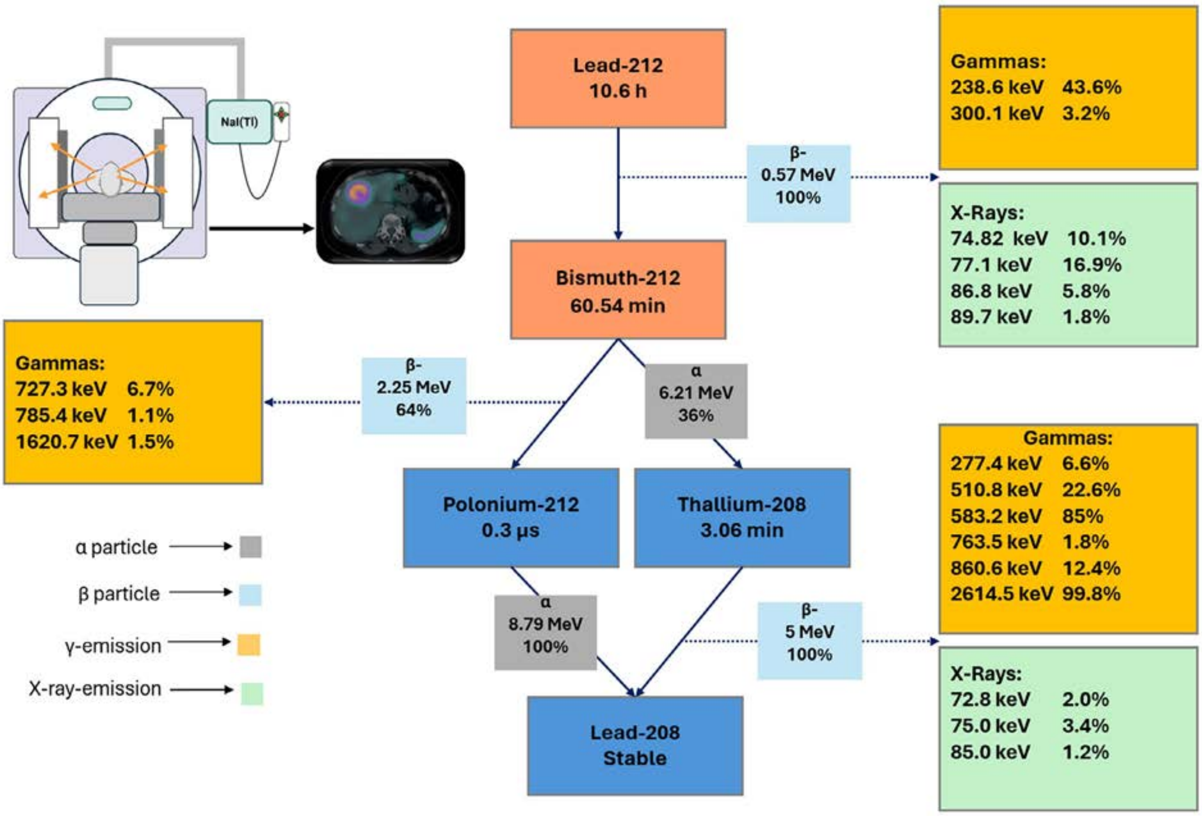

Nuclide	Daughter Nuclide (Stable)	Half-Life	Particle emissions/ Mode of decay	Particle Energy (MeV) & Intensity (%)	Imaging (keV) & Intensity (%)
^{212}Pb	^{208}Pb	10.60 h	β^- (100.0%)	0.15 (4.99) 0.33 (81.7) 0.60 (13.3)	γ: 238.63 (43.6) 300.10 (3.2) X-Rays: 74.82 (10.1) 77.10 (16.9) 86.84, 87.34, 87.68 (5.8) 89.73, 90.07, 90.42 (1.8)

Figure 2 Decay scheme of ^{212}Pb, showing mean α- and β-particle energies, along with the associated photon emissions and their respective energies.[46] Decay scheme adopted from Kvassheim et al. 2022.[47] Images adopted from Michler et al. 2025.[92]

practical balance between manageable clinical handling and effective tumor irradiation, making it logistically suitable for TAT.

The ^{203}Pb/^{212}Pb pair represents the only elementally identical theranostic combination currently available, uniquely integrating theranostic capabilities.[48] In this pair, ^{203}Pb serves as the diagnostic component, decaying via electron capture to stable ^{203}Tl (Fig. 3) and emitting 279.2 keV photons with an 80.9% abundance,[49] which are ideal for quantitative SPECT-based imaging. With a physical half-life of 51.9 h, ^{203}Pb provides an adequate timeframe to monitor radiopharmaceutical biodistribution and perform quantitative dosimetry, while its therapeutic analogue, ^{212}Pb, emits high-LET α-particles that enable highly localized tumor cell killing.[50]

Within the theranostic context, the extraordinary potency of α-particles is counterbalanced by challenges related to nuclear recoil. The extent of recoil-induced redistribution is influenced by pharmacokinetics, chelator stability, cellular

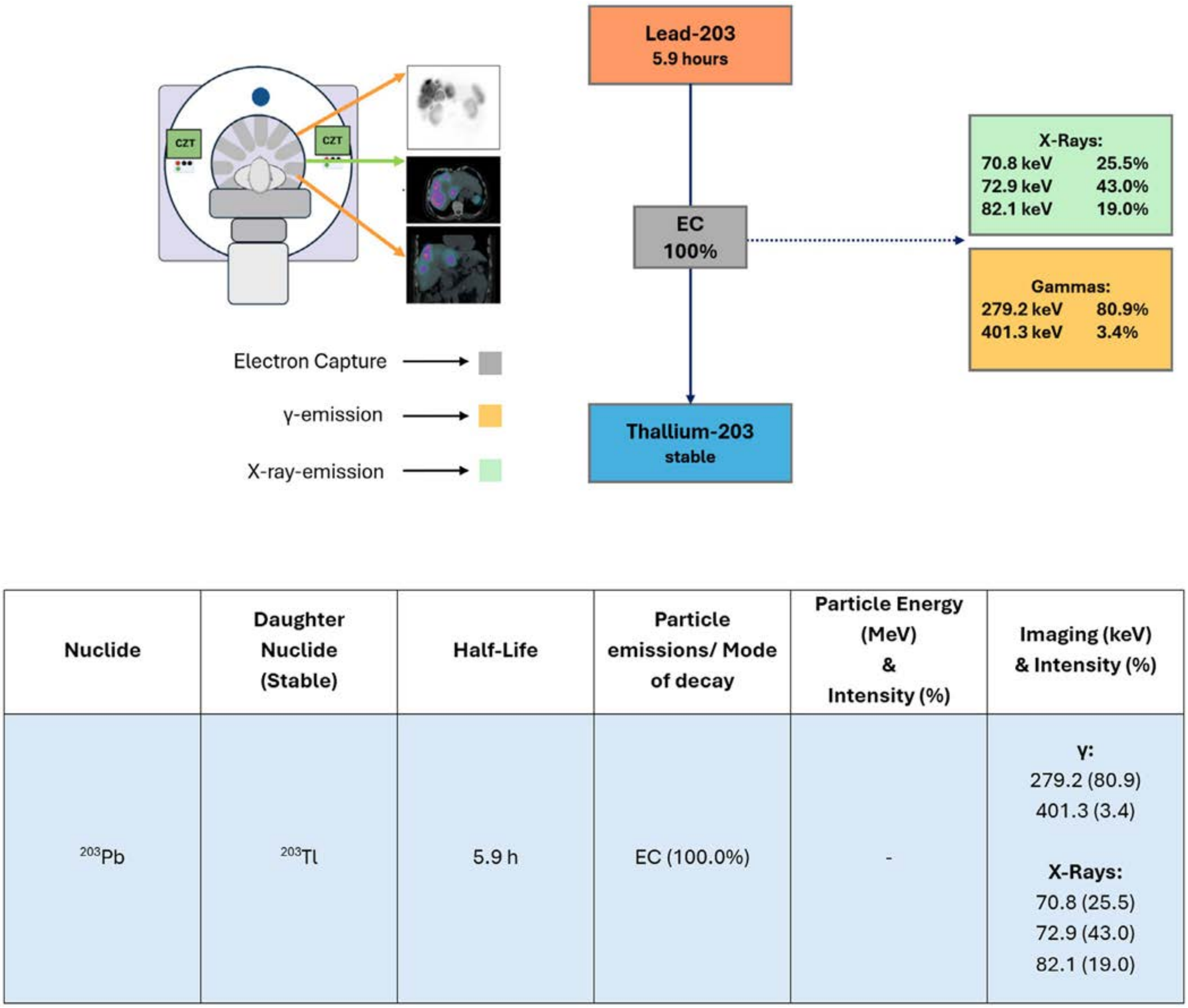

Nuclide	Daughter Nuclide (Stable)	Half-Life	Particle emissions/ Mode of decay	Particle Energy (MeV) & Intensity (%)	Imaging (keV) & Intensity (%)
^{203}Pb	^{203}Tl	5.9 h	EC (100.0%)	-	**γ:** 279.2 (80.9) 401.3 (3.4) **X-Rays:** 70.8 (25.5) 72.9 (43.0) 82.1 (19.0)

Figure 3 Decay scheme of ^{203}Pb (electron capture to ^{203}Tl), with associated γ-ray emissions and Tl characteristic X-rays indicated at each transition.[49] Decay scheme adopted from McNeil et al. 2023.[48] Images adopted from Michler et al. 2025.[92]

internalization, and inter-patient variability, emphasizing the need for radionuclides with stable chelation, predictable decay chains, and manageable daughter kinetics. These considerations are particularly relevant to the radiopharmacy and radiochemistry of ^{203}Pb and ^{212}Pb.

Theranostic Radiopharmacy and Radiochemistry of ^{203}Pb and ^{212}Pb

^{203}Pb is produced via proton irradiation of enriched ^{205}Tl targets through the ^{205}Tl(p,3n)^{203}Pb nuclear reaction.[51] High-purity [^{203}Pb]PbCl$_2$ or [^{203}Pb]Pb(OAc)$_2$ is obtained using automated systems (eg, NEPTIS Mosaic-LC), which apply Pb-selective resins such as Eichrom Pb resin. Elution with 8 M HCl or 1 M ammonium acetate yields products with high specific activity, minimal radionuclidic impurities ($<$0.1% ^{201}Pb), and $<$0.4 ppm stable Pb, suitable for direct radiolabeling.[51] Despite the high cost of enriched ^{205}Tl, increased demand for ^{203}Pb/^{212}Pb theranostic pairs is expected to incentivize broader production and optimization.[51,52]

^{212}Pb is typically obtained from ^{224}Ra/^{212}Pb generators. Traditional solid-phase ion-exchange systems utilize resins such as AGMP-50 or Sr Resin for selective Pb(II) extraction, with subsequent elution and purification.[53,54] A recently developed liquid-based generator system allows in situ labeling of biomolecules (eg, monoclonal antibodies) in radiolabeling-compatible buffers and simplifies separation using gel filtration.[55] This eliminates the need for acid elution or drying steps and supports clinical radiopharmaceutical preparation, though concerns remain regarding trace ^{224}Ra breakthrough and single-use constraints.[55]

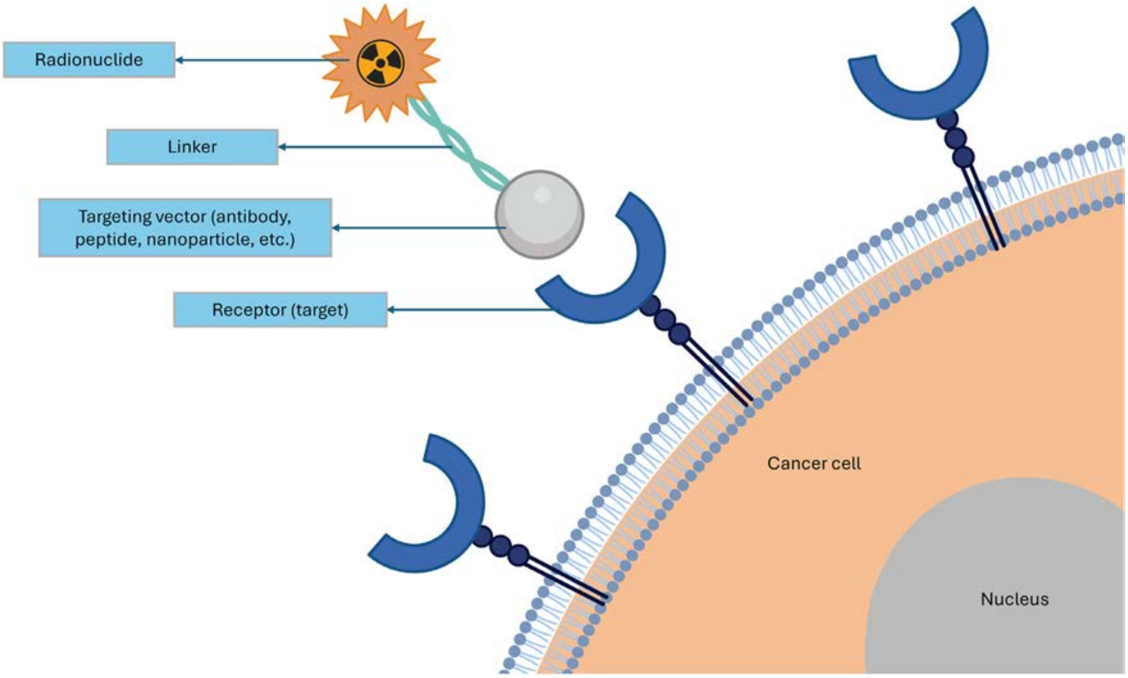

Figure 4 Conceptual illustration of targeted alpha therapy, depicting the radionuclide, targeting vector, and interaction with the intended cellular target.

Efficient chelation is essential to minimize release of daughter radionuclides (notably ^{212}Bi) after β^--decay of ^{212}Pb. DOTA and TCMC are the most widely studied chelators for ^{212}Pb.[55-57] ^{212}Pb has +2 oxidation state and forms a complexes with both TCMC and DOTA.TCMC offers superior in vivo performance, including higher complexation efficiency, greater resistance to acid dissociation, and lower ^{212}Bi release (∼30%-36% for DOTA vs. less for TCMC), contributing to reduced kidney retention and toxicity.[57] PIP-DTPA and AZEP-DTPA, cyclic derivatives of DTPA, have been evaluated with ^{203}Pb, with PIP-DTPA showing better renal clearance of ^{212}Bi, despite faster systemic clearance.[58] Azacrown ethers (eg, NOTA, TETA) and bulky ligands show poor Pb(II) coordination due to size mismatch, while newer ligands like NETA exhibit improved stability and biodistribution.[56,58]

Phosphonate-containing chelators such as DOTMP and EDTMP also form stable Pb(II) complexes, though they similarly permit ^{212}Bi release. DOTMP exhibits better in vivo stability than EDTMP but still leads to some renal accumulation.[58]

Vector selection depends on biological target, disease kinetics, and radionuclide half-life (Fig. 4). Monoclonal antibodies (mAbs), with their high specificity and prolonged circulation, may be suitable for ^{212}Pb despite the radionuclide's relatively short half-life.[59] Peptides and small molecules allow for rapid tumor targeting and clearance, aligning well with ^{212}Pb's decay window. Clinically, somatostatin analogs (eg, DOTATATE) and PSMA ligands have demonstrated excellent targeting efficacy.[60] Emerging platforms such as DARPins and miniproteins offer a promising balance between rapid kinetics and high specificity, making them attractive vectors for ^{212}Pb-based TAT, although they remain under early-stage investigation.[61]

The theranostic role of ^{203}Pb extends beyond tumor imaging to enable individualized dosimetry and pharmacokinetic profiling. As a chemically identical analog to ^{212}Pb, ^{203}Pb facilitates non-invasive quantification of biodistribution, C_max, T_max, tumor uptake, adverse effects, and radiation dosimetry, critical for treatment planning and monitoring response.[51,62] ^{212}Pb has emerged as a clinically significant radionuclide with strong therapeutic potential for receptor TAT.[63,63-65]

Clinical Applications of Targeted Alpha Therapy Using ^{212}Pb

Recent clinical trials with ^{212}Pb-labeled radiopharmaceuticals have demonstrated encouraging therapeutic efficacy.[60,66-69] These findings have intensified interest in the ^{203}Pb/^{212}Pb theranostic pair as a platform for image-guided, dosimetry-based personalized cancer therapy.[61-65] An overview of clinical trials with targeted α-therapy using ^{212}Pb is summarized in Table 1, while studies incorporating ^{203}Pb as one of the outcome measures are presented in Table 2.

Surrogate Imaging With ^{203}Pb for ^{212}Pb Targeted Alpha Therapy

The clinical application of TAT with ^{212}Pb is limited by the absence of directly imageable α-particles and the low-abundance γ emissions, which are insufficient for reliable imaging. Detectable signals instead originate from accompanying β^- and γ photons, as well as characteristic X-rays generated during

Table 1 Clinical Trials With Targeted Alpha Therapy Using ^{212}Pb:

Trial Number	Target	Agent	Setting	Primary Outcomes Measured
NCT05720130	PSMA	^{212}Pb-ADVC001	mCRPC with prior ARPI and no prior exposure to ^{177}Lu	RP2D
NCT05725070	PSMA	^{212}Pb-NG001	mCRPC with prior ARPI and no prior exposure to PSMA-targeted RLT	SPECT/CT imaging, AE
NCT03466216	SSTR2	^{212}Pb-DOTAMTATE	SSTR2-positive neuroendocrine tumors refractory to standard therapies	DLT, MTD
NCT05153772	SSTR2	^{212}Pb-DOTAMTATE	SSTR2-positive neuroendocrine tumors refractory to standard therapies	ORR, AE
NCT05636618	SSTR2	^{212}Pb-VMT-α-NET	SSTR2-positive neuroendocrine tumors refractory to standard therapies	RP2D, MTD
NCT06148636	SSTR2	^{212}Pb-VMT-α-NET	SSTR2-positive neuroendocrine tumors refractory to standard therapies	RP2D
NCT06479811	SSTR2	^{212}Pb-VMT-α-NET	SSTR2-positive neuroendocrine tumors refractory to standard therapies	DLT, MTD
NCT06427798	SSTR2	^{212}Pb-VMT-α-NET	SSTR2-positive neuroendocrine tumors refractory to standard therapies	ORR, MTD
NCT06710756	FAP	^{212}Pb-PSV359	FAP-positive solid tumors refractory to standard therapies	Safety, tolerability, antitumor efficacy
NCT05655312	MC1R	^{212}Pb-VMT-01	MC1R-positive unresectable and metastatic melanoma	ORR, AE, DLT
NCT05557708	CXCR4	^{212}Pb-Pentixather	CXCR4-positive atypical carcinoid lesions of the lung	RP2D
NCT05283330	GRPR1	^{212}Pb-DOTAM-GRPR1	GRPR1-positive solid tumors refractory to standard therapies	RP2D

Abbreviations: PSMA, prostate-specific membrane antigen; mCRPC, metastatic castration-resistant prostate cancer; ARPI, androgen-receptor pathway inhibitor; DLT, dose-limiting toxicities; MTD, maximum tolerated dose; RP2D, recommended phase 2 dose; AE, adverse events; ORR, objective response rate; SSTR2, somatostatin receptor type 2; PFS, progression-free survival; GRPR1, gastrin-releasing peptide receptor; OS, overall survival.

Table 2 Clinical Trials With Targeted Alpha Therapy Using ^{203}Pb as One of the Outcome Measures

Trial Number	Target	Agent	Setting	Primary Outcomes Measured
NCT05111509	SSTR2	^{203}Pb-VMT-α-NET	SSTR2-positive neuroendocrine tumors refractory to standard therapies	SPECT/CT tumor identification, AE
NCT5636618	SSTR2	^{203}Pb-VMT-α-NET	SSTR2-positive neuroendocrine tumors refractory to standard therapies	Biodistribution, AE, Dosimetry
NCT06479811	SSTR2	^{203}Pb-VMT-α-NET	SSTR2-positive neuroendocrine tumors refractory to standard therapies	Biodistribution, AE, Dosimetry
NCT06427798	SSTR2	^{203}Pb-VMT-α-NET	SSTR2-positive neuroendocrine tumors refractory to standard therapies	Biodistribution, AE, Dosimetry
NCT06710756	FAP	^{203}Pb-PSV359	FAP-positive solid tumors refractory to standard therapies	Biodistribution, Cmax, Tmax, AE
NCT04904120	MC1R	^{203}Pb-VMT01	MC1R-positive unresectable and metastatic melanoma	Biodistribution, AE, Cmax, Renal Excretion, Dosimetry
NCT05557708	CXCR4	^{203}Pb-Pentixather	CXCR4-positive atypical carcinoid lesions of the lung	SPECT/CT tumor identification, AE

Abbreviations: SPECT/CT, Single photon emission tomography/computed tomography; DLT, dose-limiting toxicities; MTD, maximum tolerated dose; RP2D, recommended phase 2 dose; AE, adverse events; ORR, objective response rate; SSTR2, somatostatin receptor type 2; PFS, progression-free survival; GRPR1, gastrin-releasing peptide receptor; OS, overall survival.

decay and from daughter radionuclides. To enable molecular imaging, predictive dosimetry, and individualized treatment planning, radionuclides with more abundant and quantifiable photon emissions, are employed as surrogates.

Surrogate imaging has historically relied on positron emitters, leveraging the high sensitivity, resolution, and quantitative accuracy of PET. Accordingly, Gallium-68 (^{68}Ga), Fluorine-18 (^{18}F), Copper-64 (^{64}Cu), Zirconium-89 (^{89}Zr) and Iodine-124 (^{124}I) remain widely used imaging counterparts in clinical theranostics. In contrast to PET-based surrogates, SPECT can directly utilize γ emissions from therapeutic radionuclides, allowing continuous monitoring of treatment response without the need for additional imaging agents.[70]

The rationale for elementally matched surrogates, such as ^{203}Pb/^{212}Pb is supported by comparative studies demonstrating pharmacokinetic discrepancies between chemically distinct isotope pairs (eg, ^{68}Ga- vs. ^{90}Y-labeled peptides).[71] As an isotope of the same element, ^{203}Pb exhibits identical coordination chemistry and biological behavior to ^{212}Pb while providing favorable photon emissions (279 keV (80.9%)) suitable for quantitative SPECT and SPECT/CT imaging.[10,63,72] Its longer half-life (51.9 h) further supports extended pharmacokinetic studies and improved dosimetry accuracy, advantages not achievable with short-lived PET isotopes such as ^{68}Ga.

Despite these strengths, important uncertainties remain when translating ^{203}Pb imaging to ^{212}Pb therapy. Leading among these is the in vivo stability of the ^{212}Pb-ligand complex and the potential redistribution of its α-emitting progeny (^{212}Bi, ^{212}Po). Such redistribution can create discrepancies between the imaging profile of ^{203}Pb and the absorbed dose distribution of ^{212}Pb and its daughters. Resolving these uncertainties requires systematic investigation of complex stability, progeny retention, and correlation of absorbed dose estimates with biological outcomes.

Within this theranostic paradigm, ^{203}Pb provides a scientifically robust platform for quantitative SPECT-based dosimetry, supporting accurate biodistribution studies, pharmacokinetic characterization, and treatment optimization of ^{212}Pb-labeled radiopharmaceuticals. Its use exemplifies the theranostic principle, wherein an elementally matched diagnostic partner yields clinically actionable data to guide and personalize TAT. Figures 2 and 3 summarize the key γ and X-ray emissions of ^{203}Pb, ^{212}Pb, and their progeny, emphasizing the imaging characteristics most relevant for dosimetry. These decay emissions also inform and facilitate the optimization of recommended acquisition protocols for quantitative SPECT imaging with ^{203}Pb and ^{212}Pb.

Clinical SPECT Gamma Cameras: Dual-Head and CZT Multi-Detector Systems

The acquisition protocols for SPECT imaging in TAT are fundamentally dictated by gamma camera performance. Key system parameters, including energy resolution, spatial resolution, and sensitivity, directly shape image quality, quantitative accuracy, and clinical feasibility. High energy resolution enables narrower energy windows for improved scatter discrimination, while enhanced spatial resolution facilitates the detection of small, clinically relevant lesions near the system's resolution limit[73]. Sensitivity governs acquisition times, which is particularly critical for whole-body SPECT/CT studies required for individualized dosimetry, where optimized systems reduce scan duration, improving patient comfort and clinical throughput.

Traditional NaI(Tl)-based scintillation detectors, although cost-effective and widely available, are limited by their reliance on photomultiplier tubes (PMTs). The multiple photon-to-electron conversion steps introduce statistical uncertainties in both energy measurement and spatial localization, limiting quantitative accuracy and spatial fidelity.[74] The key performance characteristics of the SPECT/CT systems are summarized in Table 3.

Solid-state Cadmium Zinc Telluride (CZT) detectors overcome these limitations (Fig. 5), to a certain extent, by directly converting incident γ photons into electrical signals via charge induction from photoelectric and Compton interactions. The absence of PMTs reduces statistical uncertainty, improving spatial resolution to ~2-3 mm.[79] Pixelated CZT detector designs effectively reduce dead-time losses and signal saturation, while permitting closer detector positioning. By eliminating edge distortions and expanding the usable field of view, these systems significantly enhance lesion detectability and quantitative reliability, making them especially valuable for post-therapy imaging of ^{203}Pb and ^{212}Pb.[75]

Commercially available 3D-ring CZT SPECT/CT systems, by Spectrum Dynamics' Veriton and GE Healthcare's StarGuide extend early cardiac CZT[80,81] designs to whole-body imaging, enabling dynamic and rapid acquisitions for theranostic applications. The Veriton-CT 200 series features twelve independently swiveling digital detector columns arranged in a full 360° ring, with adaptive body contouring to minimize detector-to-patient distance and maximize sensitivity and spatial resolution. The SPECT energy range for the Veriton is 40-200 keV. Each column can move radially, rotate along the gantry, and sweep, supporting flexible, patient-adapted acquisition protocols.

The StarGuide SPECT/CT system similarly employs twelve detector columns, each comprising seven 16×16 CZT pixelated modules (2.46×2.46 mm^2, 7.25 mm thick) with dual-pitched tungsten parallel-hole collimators aligned to each pixel. StarGuide operates over a wider energy range of 40-279 keV in 2 modes: a "low energy" mode (channels = 0.5 keV) for energies up to 200 keV, and a "medium energy" mode (channels = 1 keV) for peaks above 200 keV, accommodating the primary γ emissions of ^{203}Pb at 279 keV (80.9%) and ^{212}Pb at 238.6 keV (43.3%). The extended energy range also accommodates scanning of photon energies up 500 keV. Each column moves independently with radial, rotational (2-6 steps per bed position, rotation up to 25°), and sweep (±15°) motions, allowing high temporal resolution and patient-adapted acquisitions.

Table 3 Comparison of Fundamental Performance Characteristics of Conventional, Digital, and Multidetector 3-Dimensional CZT SPECT/CT Systems

Parameter	Conventional NaI(Tl)	Digital CZT SPECT	Multidetector 3D CZT SPECT/CT
Spatial resolution (FWHM)	≈22 mm (MEGP)[75]	≈10 mm (MEGP)[1]	≈ 3 mm (pixelated CZT, adaptive body contouring)[76]
System sensitivity (cps/MBq)	^{203}Pb (78,8 on MELP collimator and 43.2 keV on HE collimator for 279 keV photopeak) ^{212}Pb (1148.9 on MELP collimator and 622.7 on HE collimator for 239 keV photopeak)[77]	-	-
Energy Range (keV)	30-360 (typical range)[78]	40-250[6]	40-200 (Veriton series dependent) 40-200: Low Energy Range & 40-500: Extended energy range (StarGuide)[76]
Whole-body acquisition time[1]	30-40 min	20 min	12-15 min (patient adapted, high sensitivity)
Quantitative accuracy (typical limits)[1]	± 10%	± 5%	± 5%

Both Veriton and StarGuide provide high-resolution, quantitative imaging, rapid whole-body SPECT, dynamic acquisition protocols, and patient-friendly scan durations, supporting the requirements of individualized dosimetry and post-therapy monitoring in ^{203}Pb/^{212}Pb-TAT. The specific energy range used for acquisition must be carefully selected based on the camera series, as this directly influences the accurate detection of the primary γ emissions and characteristic X-rays of each radionuclide. Although neither system currently allows collimator exchange, it is essential to account for septal penetration effects and apply, where appropriate, corrections during image reconstruction to maintain quantitative accuracy.

SPECT system performance varies substantially across designs, as shown in Table 3, with direct implications for acquisition protocols in dosimetry. Conventional NaI(Tl)-based SPECT systems typically achieve a spatial resolution of ∼22 mm with a MEGP collimator. Kästner et al[77] reported sensitivities of 78.8 cps/MBq (MELP) and 43.2 cps/MBq (HE) for the 279 keV photopeak of ^{203}Pb, and 1148.9 cps/MBq (MELP) and 622.7 cps/MBq (HE)

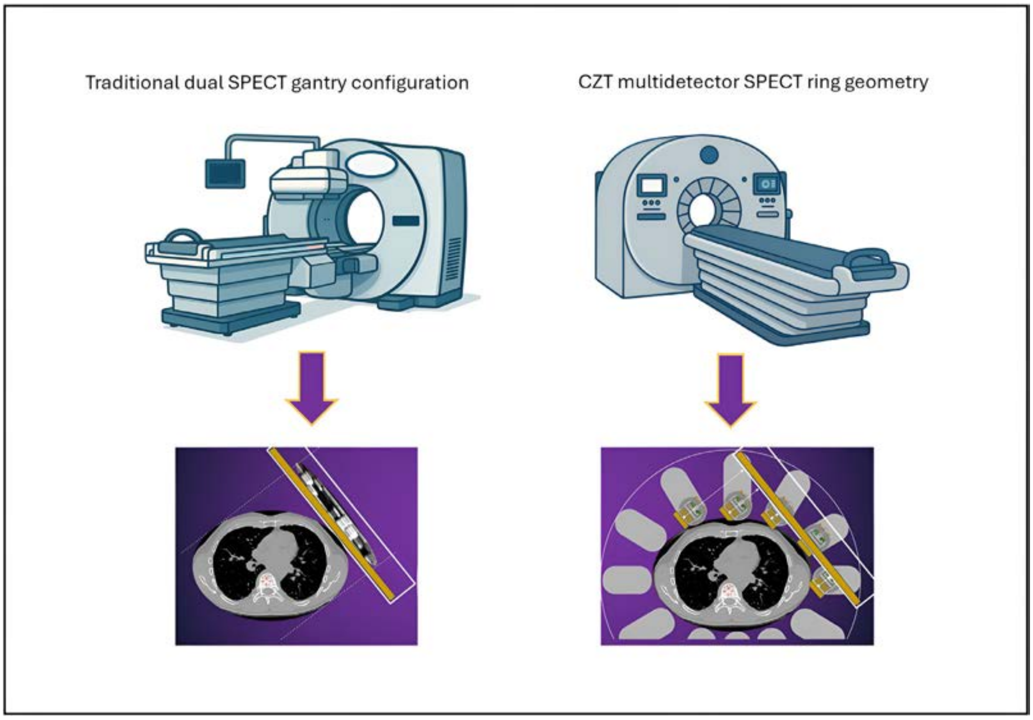

Figure 5 Comparison between traditional dual-head SPECT gantry configuration and the advanced CZT ring geometry enabling fully 3D multidetector acquisition. GE Healthineers.

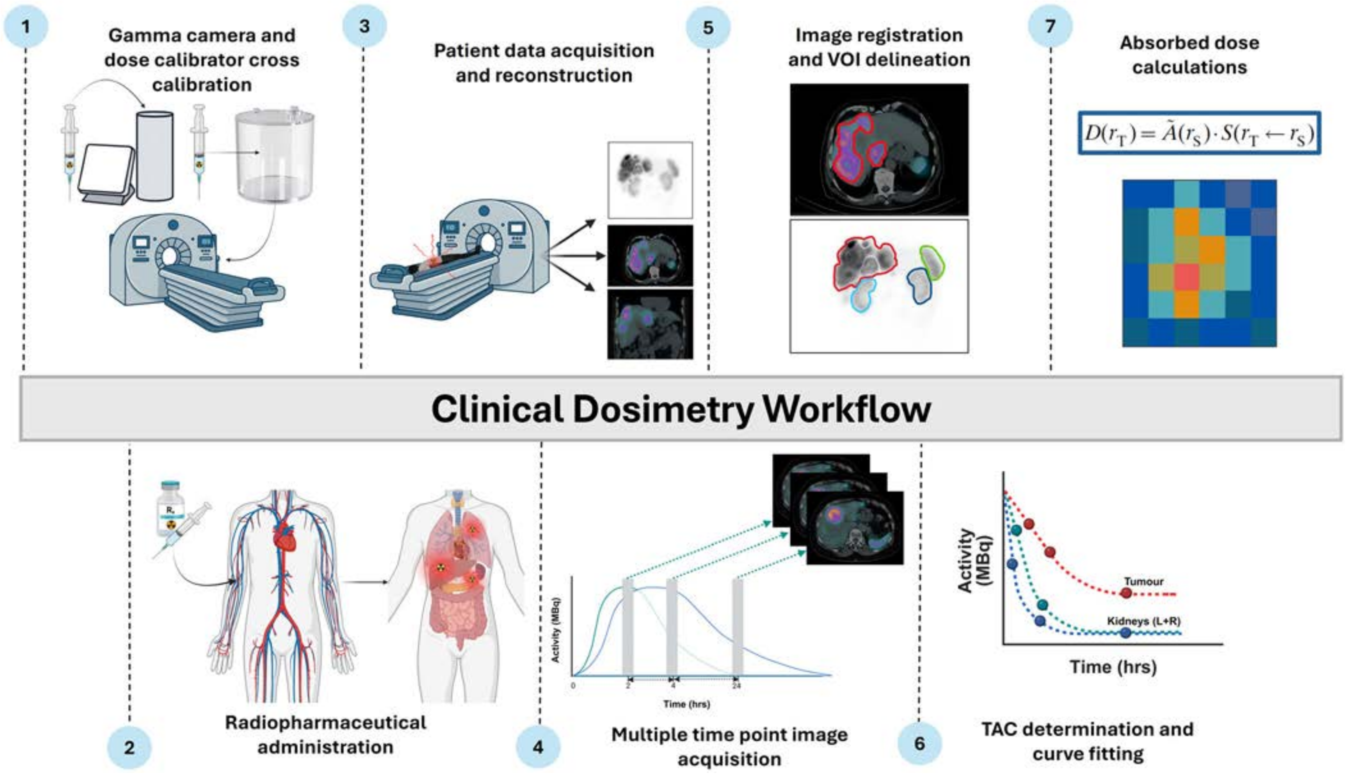

Figure 6 Serial steps in clinical image-based dosimetry workflow for targeted radionuclide therapy. Images adopted from Michler et al. 2025.[92]

for the 239 keV photopeak of ^{212}Pb. Whole-body acquisitions on these systems typically require 30-40 minutes, with quantitative accuracy within ±10%. Digital dual-head CZT SPECT and multidetector 3D CZT SPECT/CT systems offer marked improvements, providing spatial resolutions (FWHM) of ~10 mm and ~3 mm, respectively. Although sensitivity data for ^{203}Pb and ^{212}Pb on CZT systems remain under investigation, their performance in terms of sensitivity, may surpass that of NaI(Tl)-based cameras, particularly in 3D ring geometries. These advances enable reduced acquisition times of ~20 minutes for dual-head CZT and 12-15 minutes for 3D CZT SPECT/CT while improving quantitative accuracy to within ±5%. Together, these performance characteristics, ie, spatial resolution, sensitivity, and acquisition speed, critically inform optimized acquisition protocols. Consequently, SPECT imaging, whether conventional, CZT, or multidetector 3D, forms an integral component of the clinical dosimetry workflow, where accurate quantitative imaging supports patient-specific planning and treatment optimization in TAT.

Clinical Dosimetry Workflow

Accurate clinical dosimetry is fundamental for optimizing patient outcomes and minimizing uncertainties in both routine practice and clinical trials. By enabling patient-specific treatment planning, it maximizes tumor dose delivery while maintaining safe margins for normal tissues, thereby overcoming the limitations of fixed-activity protocols, in which normal tissue exposure may vary up to 5-fold per administered activity.[82] Dosimetry-guided TRT not only improves survival and therapeutic efficacy but also provides essential data to establish absorbed dose thresholds and to define tumor- and organ-specific dose−response relationships. In addition, it facilitates cross-comparisons of different radiopharmaceuticals across patient populations, ultimately strengthening the foundation for evidence-based TRT planning. The dosimetry workflow in TRT consists of a series of fundamental steps designed to achieve accurate, patient-specific absorbed dose estimates for both target lesions and normal organs (Fig. 6).

The process begins with accurate activity measurement using a dose calibrator, followed by the gamma camera calibration to establish radionuclide and acquisition protocol-specific calibration factors (CFs). This relies on serial SPECT/CT imaging to capture the spatio-temporal distribution of activity with improved quantitative accuracy, ensuring reliable dosimetric assessment. The resulting images undergo reconstruction with corrections for attenuation, scatter, collimator-detector response, and partial-volume effects, and, where applicable, dead-time corrections, to enable absolute activity quantification. Registration and segmentation of volumes of interest (VOIs) across multiple time-points are subsequently performed, increasingly supported by AI-based tools. From these data, time−activity curves (TACs) are generated, fitted, and integrated to determine time-integrated activity (TIA), with careful control of extrapolation to minimize error. Finally, absorbed dose calculation is performed either through Medical Internal Radiation Dose (MIRD) formalism using S-values or via patient-specific methods such as voxel-based approaches and direct Monte Carlo (MC) simulations, the latter providing the highest level of accuracy by accounting for tissue heterogeneity and non-uniform activity distributions. Details regarding these fundamental steps in the image-based dosimetry workflow were comprehensively outlined in our previous publication.[83]

Within the dosimetry workflow, the subsequent sections focus on key aspects of TAT dosimetry,[84] with particular emphasis on ^{203}Pb and ^{212}Pb. (1) Pharmacokinetics and activity quantification: Accurate activity quantification is essential for deriving reliable pharmacokinetic data, as errors in biodistribution measurements propagate directly into absorbed dose estimates. (2) Daughter radionuclides: Accurate dosimetry requires accounting for the redistribution and migration of radioactive daughters. (3) Small-scale and microdosimetry: Given the short range and heterogeneous energy deposition of α-particles, small-scale dosimetry is needed to quantify non-uniform dose distributions at the tissue, organ, or cellular level, thereby improving predictions of biological effects.

Pharmacokinetics and Image Activity Quantification

Pharmacokinetics determine the residence times of activity within tumors and normal organs, necessitating serial quantitative imaging to construct TACs. SPECT/CT with ^{203}Pb or ^{212}Pb provides 3D distributions of activity at multiple time points, from which absorbed doses can be retrospectively calculated and prospectively applied for treatment planning. The image acquisition protocols for ^{203}Pb and ^{212}Pb are summarized in Table 4, incorporating both manufacturer-recommended settings and protocols reported in the literature[47,77] for clinical gamma cameras with CZT multi-detectors or NaI (Tl) detectors. These guidelines account for gamma camera performance characteristics, including energy resolution, as well as recommended collimator types appropriate for the energies of the imageable radiation. Although clinical imaging data using multi-detector CZT-based gamma cameras for ^{203}Pb and ^{212}Pb are not yet published, several studies have investigated optimal acquisition parameters, including the selection of medium-energy (ME) versus high-energy (HE) collimators.[47,77]

Collimator selection is a key factor influencing sensitivity, image quality, and quantitative accuracy in ^{203}Pb and ^{212}Pb imaging. A paradox has been observed: despite its lower gamma and X-ray emission probabilities, ^{212}Pb often shows higher measured sensitivity than ^{203}Pb. This phenomenon has been attributed to collimator-induced lead X-rays, septal penetration, and down-scatter from high-energy progeny emissions, particularly the 2.6 MeV photons from ^{208}Tl[77]. Collectively, published data indicate a trade-off in the imaging of the ^{203}Pb/^{212}Pb theranostic pair: MELP collimators provide superior sensitivity but are more vulnerable to septal penetration and dead-time losses, whereas HE collimators, though less sensitive, appear more reliable for quantitative ^{212}Pb imaging at therapeutic activity levels.[47,77,86] For ^{203}Pb, MELP collimators remain suitable for clinical use, while for ^{212}Pb, HE collimators are generally recommended to minimize quantification errors. Additionally, it has been noted that dead-time losses are higher in the X-ray energy window compared with the photopeak, emphasizing the importance of careful window selection.

From Table 4, ^{203}Pb emits an abundant 279 keV photon (80.9%) with minimal higher-energy contaminants (3.4% at 401.3 keV and low-abundance X-rays $<$100 keV), rendering it well-suited for quantitative SPECT.[82] Another key advantage of ^{203}Pb as a surrogate for ^{212}Pb is its sufficiently long physical half-life, exceeding 4 half-lives of its therapeutic analogue. These properties make ^{203}Pb highly suitable for quantitative imaging, activity quantification, and absorbed-dose estimation.[62,87,88]

^{212}Pb also provides measurable photon emissions through its decay to ^{212}Bi, most notably the 238.6 keV γ-ray (43.3%) and characteristic X-rays in the 75.1-87.7 keV range (36%). These emissions have been successfully employed in both preclinical and clinical studies[89,90] demonstrating the feasibility of quantitative imaging with ^{212}Pb.

For ^{203}Pb, studies report a near-linear detector response up to ∼900 MBq with $<$10% count losses, covering the diagnostic activity range of 200-500 MBq.[62,86] In contrast, ^{212}Pb is strongly affected by dead-time, with ∼20% count losses at activities as low as 20-40 MBq depending on collimator choice.[91] Consequently, dead-time correction is particularly critical at the first post-administration imaging time point, where activities are highest, and should be tailored to the count rate performance of the specific gamma camera system.

Figure 7 illustrates a comparison of image acquisitions using ^{203}Pb and ^{212}Pb, highlighting differences in image quality on SPECT/CT transverse slices, as well as in planar whole-body scans. The observed variations in image quality can be attributed to the combined effects of physical decay properties and detector-specific characteristics described above. Septal penetration and lead X-ray generation from the high-energy emissions of ^{212}Pb and its progeny contribute to increased background and spatial blurring.[92] In addition, extensive down-scatter from high-energy photons (such as the 2.6 MeV emission of ^{208}Tl) contaminates the lower-energy windows, further degrading contrast. At early time points, high activity levels may also induce dead-time losses and pulse pile-up, leading to nonlinear count recovery and spectral distortion, particularly in narrow X-ray windows, resulting in blurring and reduced contrast compared with ^{203}Pb.[77] These observations, supported by phantom studies, indicate that HE collimators provide the best balance of sensitivity and image quality for ^{212}Pb. HE collimator 79 keV images allowed the most reliable visualization of phantom spheres at lower activity concentrations, despite greater attenuation effects.[77] Taken together, these findings confirm that clinical ^{212}Pb acquisition is feasible when all image-degrading factors are accounted for through appropriate corrections and optimal collimator selection.[47]

Table 4 Recommended Image Acquisition Protocols for ^{203}Pb and ^{212}Pb Using NaI (Tl) and CZT Multi-Detector Gamma Cameras, Including Manufacturer Guidance, and Literature-Based Parameters for Collimator Selection, Energy Window Settings, and Imaging Performance Consideration

Nuclide	Daughter Nuclide (Unstable)	Gamma/ X-Ray energy (keV) and intensity (%)	Recommended SPECT Imaging Protocols	
			 CZT Multi-Ring Detector Gamma Camera	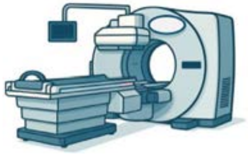 NaI(Tl) Detector Gamma Cameras
Pb-203	-	γ: 279.2 (80.9) 401.3 (3.4) X-Rays: 70.8 (25.5) 72.9 (43.0) 82.1 (19.0)	Energy windows: [Peak and Full Window Width] Emission window 1: 71 keV (20.5%) Lower scatter window 1: 63 keV (6%) Higher scatter window 1: 86 keV (14%) Emission window 2: 279 keV (12%) Lower scatter window 2: 245 keV (14%) Higher scatter window 2: 312 keV (10%) Collimator type: Intrinsic tungsten collimators (low to medium energies) Scatter correction: Window-based (TEW scatter correction)	Energy Windows: [Peak and Full Window Width] Recommendation 1(85) Primary window: 279.2 keV (20%) Lower scatter window: 239.3 keV (10%) Higher scatter window: 323.3 keV (10%) Secondary window: 72.9 keV (20%) Collimator type: MEGP Scatter correction: Model-based Recommendation 2[77] Primary window: 279 keV (20%) Lower scatter window (primary): 237 keV (10%) Higher scatter window (primary): 321 keV (10%) Secondary window: 72 keV (40%) Lower scatter window: 50 keV (20%) Higher scatter window: 97 keV (20%) Collimator type: MELP & HE
Pb-212	-	γ: 238.6 (43.6) 300.1 (3.2) X-Rays: 74.82 (10.1) 77.1 (16.9) 86.8 (5.8) 89.7 (1.8)	Energy windows: [Peak and Full Window Width] Emission window 1: 76 keV (10%) Lower scatter window 1: 70 keV (6%) Higher scatter window 1: 88 keV (14%) Emission window 2: 239 keV (10%) Lower scatter window 2: 215 keV (14%) Higher scatter window 2: 265 keV (10%) Collimator type: Intrinsic tungsten collimators (low to medium energies)	Energy windows: [Peak and Full Window Width] Recommendation 1[85] Primary window: 238.63 keV (20%) Secondary window: 76.1 keV (20%) Scatter correction: Model-based Recommendation 2[47,77] Primary window: 239 keV (20%) Lower scatter window (primary): 209 keV (5%) Higher scatter window (primary): 268 keV (5%)

Table 4 (*Continued*)

			Recommended SPECT Imaging Protocols	
Nuclide	**Daughter Nuclide (Unstable)**	**Gamma/ X-Ray energy (keV) and intensity (%)**	 **CZT Multi-Ring Detector Gamma Camera**	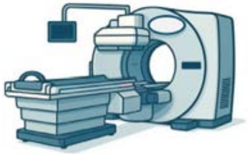 **NaI(Tl) Detector Gamma Cameras**
			Scatter correction: Window-based (TEW)	Secondary window: 79 keV (40%) Lower scatter window (secondary): 55 keV (20%) Higher scatter window (secondary): 103 keV (20%) Collimator type: MELP & HE Scatter correction: Window-based (TEW)
	Bi-212 (Unstable)	γ: 727.3 (6.7) 785.4 (1.1) 1620.7 (1.5)		
	Po-212 (Unstable)	-		
	Tl-208 (Unstable)	γ: 277.4 (6.6) 510.8 (22.6) 583.2 (85.0) 763.5 (1.8) 860.6 (12.4) 2614.5 (99.8) X-Rays: 72.8 (2.0) 75.0 (3.4) 85.0 (1.2)		

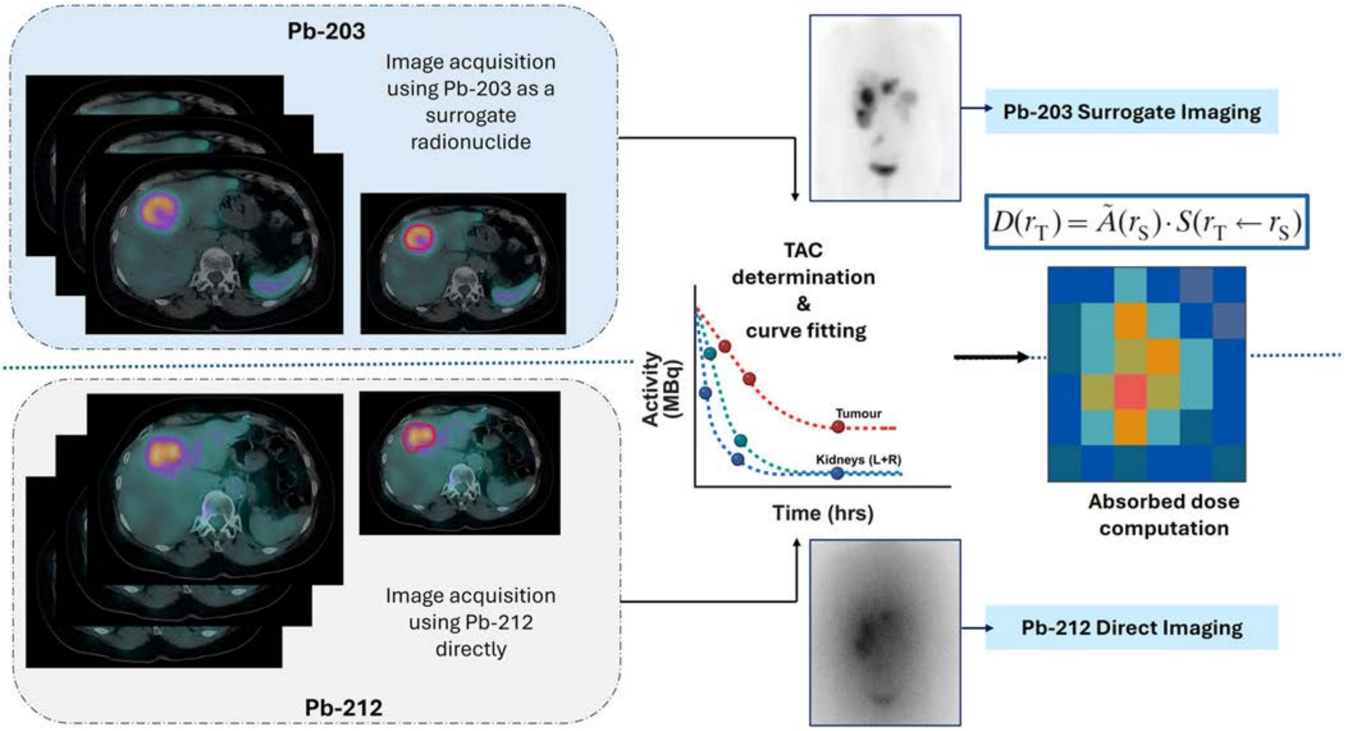

Figure 7 Comparison of image acquisition using ^{203}Pb as a surrogate radionuclide and ^{212}Pb as the direct therapeutic radionuclide. Planar whole-body scans and transversal slices are shown to illustrate differences in image quality and resolution between surrogate and direct imaging. Images adopted from Michler et al. 2025.[92]

Optimal Imaging Time Points for ^{203}Pb: Accurate dosimetry relies on quantifying organ and tumor activity across multiple time points to capture the dynamics of radiopharmaceutical distribution and clearance. Optimal imaging for ^{203}Pb dosimetry is typically performed between one and four hours post-injection, providing the best balance of tumor contrast, signal-to-noise ratio, and image quality.[92] Early acquisitions (<1 hour) capture initial biodistribution, while later time points (24-48 hours) can enhance tumor-to-liver contrast but are limited by higher noise and reduced lesion detectability.[93] Intermediate scans at 1.5-2 hours and 22 hours have also been shown to reliably reflect pharmacokinetics and support planning for subsequent ^{212}Pb therapy.[94] These findings support a flexible imaging schedule emphasizing early to intermediate time points for routine dosimetry, with later acquisitions applied selectively for low-contrast lesions or detailed pharmacokinetic analysis.

Optimal Imaging Time Points for ^{212}Pb: Phantom studies for ^{212}Pb dosimetry demonstrate reliable activity quantification at 1, 24, and 48 hours post-administration, with iterative reconstruction convergence ensuring quantitative accuracy.[95] Clinical SPECT/CT imaging following 60 MBq ^{212}Pb-ADVC001 has been successfully performed at 1.5, 5-, 20-, and 28-hours post-infusion, providing practical and feasible time points for dosimetry.[50] These findings support a flexible imaging schedule emphasizing early to intermediate scans to optimize quantitative assessment for TAT. Furthermore, the development of a ^{212}Pb quantitative SPECT/CT imaging approach, which incorporates corrections (attenuation, scatter, and CDR) for all major physical image-degrading effects, demonstrates that accurate quantitative imaging of ^{212}Pb is feasible.

Calculation of Cumulated Activity: After registration and segmentation, the activity within source regions at discrete imaging time points is quantified, enabling calculation of the cumulated activity ($\tilde{A}_{r_s}$) for each region. To generate continuous TACs, $A_{r_s}(t)$, from these discrete measurements, analytical fitting, commonly using sums of exponentials, or linear interpolation (trapezoidal method) is employed.[96]

$$A_{r_s}(t) = \sum_j A_j(0)e^{-(\lambda+\lambda_j)t} \qquad (1)$$

where $A_j(0)$ is the initial activity of the j^{th} component, λ is the physical decay constant of the radionuclide, λ_j is the biological elimination constant, and $\lambda + \lambda_j$ represents the effective elimination constant.

Appropriate extrapolation beyond the first and last image time points is critical for accurate TIA estimation, with the EANM recommending that the contribution from extrapolated intervals remain below 20% of the total TIA.[97] Integration can be performed at the organ level, assuming homogeneous kinetics, or at the voxel level to capture heterogeneous distributions relevant to microdosimetry. This approach forms the basis for predictive ^{212}Pb dosimetry using ^{203}Pb SPECT imaging.

Predictive ^{212}Pb Dosimetry Using ^{203}Pb SPECT/CT Imaging

^{212}Pb decays to ^{212}Bi via beta emission, imparting relatively low recoil energy to the daughter nucleus and thus reducing the likelihood of dissociation from the chelator.[87] Nevertheless, migration of ^{212}Bi from the site of ^{212}Pb decay remains a critical determinant of dosimetric accuracy, as the alpha emissions from ^{212}Bi and ^{212}Po contribute most of the therapeutic dose. Empirical data indicate that up to ~36% of ^{212}Bi can be lost from the targeting vector,[98] highlighting the need to account for daughter redistribution when extrapolating from ^{203}Pb-derived pharmacokinetics.

Limited studies have evaluated the kinetic stability of ^{212}Bi across different chelator-ligand systems. In vitro data suggest that approximately 30% of ^{212}Pb decays can release ^{212}Bi from certain DOTA derivatives lacking peptide ligands, representing a significant source of uncertainty for pre-treatment dosimetry based on ^{203}Pb imaging.[98,99] Pharmacokinetic modeling incorporating human bismuth biokinetics further demonstrates that redistribution of released ^{212}Bi to the plasma, liver, and kidneys can occur rapidly, potentially leading to overestimation of tumor dose and underestimation of dose to normal tissues if ignored.

To address these challenges, generalized correction formalisms have been proposed in which ^{203}Pb-derived time-integrated activities (TIAs) are adjusted for daughter redistribution using experimentally or model-derived fractions of bismuth release (f) and organ-specific decay probabilities $\psi(r_i \leftarrow r_s)$. Such approaches enable a more accurate prediction of ^{212}Pb TIA and improve patient-specific dosimetry while preserving the spatial fidelity of tumor versus normal tissue dose. TAC-derived TIAs must be corrected for potential redistribution of ^{212}Bi generated by ^{212}Pb.

If the fraction of released bismuth ions (f) is known, a generalized formalism can adjust the ^{203}Pb-derived TIA:[87]

$$A_{(r_i)} = (1 - f)A_{raw}(r_i) + f\sum_{r_s} A_{raw}(r_s)\psi(r_i \leftarrow r_s) \quad (2)$$

Where $A_{raw}(r_i)$ is the TIA for a given organ (r_i) without correcting for the redistribution effect and $A(r_i)$ is the corrected TIA for that organ. The fractional transfer of TIA from a given source organ (r_s) to the organ of interest (r_i) is represented by the product of f and $\psi(r_i \leftarrow r_s)$where $\psi(r_i \leftarrow r_s)$describes the probability of a given bismuth ion decaying in r_i when it was released from r_s. The additive correction $\sum_{r_s} A_{raw}(r_s)\psi(r_i \leftarrow r_s)$ allows for the uniform distribution of TIA in all soft tissue, including tumors.

Incorporating microdosimetric corrections and sub-organ pharmacokinetic models allows refinement of absorbed dose estimates while accounting for daughter nuclide migration, redistribution, and chelator stability. Continuous TAC fitting and extrapolation generate corrected TIA for all organs. Using these data, patient-specific dosimetry can be performed according to MIRD principles.[100]

Absorbed Dose Estimation

Several approaches exist for converting cumulated activities ($\tilde{A}_{rs}$) into absorbed dose. The MIRD formalism, established by the MIRD Committee of the Society of Nuclear Medicine, was the first widely adopted dosimetric framework. It enables calculation of mean absorbed doses in source and target regions by combining time-integrated activities with precomputed S-values, which represent the mean dose per unit cumulated activity from a source region to a target region.[100]

$$D(r_T) = \sum_{r_s} \tilde{A}_{r_s} \cdot S(r_T \leftarrow r_s) \quad (3)$$

Where; $D(r_T)$represents the absorbed dose delivered to the target region r_T, (A_{rs}) is the TIA in the source region r_s and S $(r_T \leftarrow r_s)$ or S-value, denotes the mean absorbed dose in r_T per unit of activity present in r_s.

Methods for computing S-values include local energy deposition (LDM), dose-point kernels (DPK), and MC simulations. While the classical MIRD approach assumes uniform activity distribution and homogeneous tissue, it remains widely used due to its speed and ability to incorporate planar imaging. Patient-specific dosimetry methods leverage voxelized S-values and dose maps, producing dose—volume histograms (DVHs) for organs and lesions.

MC simulations explicitly model decay locations and radiation transport within patient-specific geometry derived from CT, providing accurate voxel-level energy deposition. DPKs can be discretized over source and target voxels to generate dose maps via convolution with cumulated activity, while voxel S-values (VSVs) extend MIRD principles to the voxel scale. LDM assumes complete energy absorption within the source voxel, making it appropriate for alpha or short-range beta emitters. Although DPK and VSV may underestimate dose in heterogeneous tissues, MC simulations or LDM may be preferred depending on image resolution and computational resources. A detailed description of these methods has been provided in our previous publication.[83] Collectively, these approaches enable estimation of ^{212}Pb dosimetry for TAT, accounting for physical, biological, and microdosimetric factors. This framework provides a robust foundation for patient-specific dosimetry and can be extended to voxel-level or microdosimetric analyses when activity distributions are heterogeneous.

Small-scale and Microdosimetry With Emphasis on ^{212}Pb-based Targeted Alpha Therapy

For ^{212}Pb TAT, conventional organ-level dosimetry based on the MIRD formalism provides a first approximation but is insufficient to capture the biological effects of short-ranged, high-LET alpha particles. Microdosimetry addresses the

Table 5 Targeted Alpha Therapy Multiscale ^{212}Pb Dosimetry Studies

Macrodosimetry

Radiopharmaceutical	Objective	Dosimetry Methodology	Findings	Reference number
^{212}Pb-MC1L	Assessment of renal dosimetry	Analytic: OLINDA/MIRD	Kidney absorbed doses reached 2.8-20 Gy, depending on ^{212}Pb-MC1L injected activity; high doses induced CKD and histological damage	102
^{212}Pb-CA012 and ^{203}Pb-CA012	Assessment of effective dose estimates using ^{203}Pb-CA012 imaging to simulate ^{212}Pb-CA012 uptake	Analytic: OLINDA/QDOSE	The estimated effective dose was 2.4± 0.3 mSv/100Mbq when ^{203}Pb-CA012 was administered. The projected effective dose was 415.1±13.5 mSv/100Mbq for ^{212}Pb-CA012.	62
^{212}Pb-VMT01 and ^{203}Pb-VMT01	Assessment of renal and bone marrow dosimetry using ^{203}Pb-VMT01 and ^{212}Pb-VMT01, and the impact of the accumulation of free 208Tl	Analytic: OLINDA/EXM2.0	Kidney absorbed doses reached 8.27 mGy/Mbq, depending on ^{212}Pb-VMT01 injected activity, and the red bone marrow reached 1.06 mGy/Mbq. The highest increased percentage dose distribution from 208Tl was 2.1% for the brain.	103
^{212}Pb-rhPSMA, 225Ac- rhPSMA and ^{177}Lu- rhPSMA	Assessment of renal dosimetry and therapeutic indices (TI) using 225Ac and ^{212}Pb modeled data from ^{177}Lu dosimetry data	Analytic: MIRD/LabPlot 2.10.0	A 29-fold higher dose of 212Pb was required to achieve the same therapeutic outcome as 225Ac. 225Ac showed a 2.5 factor decrease in the absorbed dose to the kidneys and 2.2 factor decrease in the absorbed dose to the salivary glands as compared to ^{212}Pb. The TI for tumour: kidney dose ratio was 3-fold higher for 225Ac than ^{212}Pb as compared to the modeled data.	104
Microdosimetry				
^{212}Pb-anti HER2	Improvement of TAT cellular dosimetry accuracy by incorporating realistic cell morphology, binding kinetics, and stochastic radiation effects	Monte Carlo microdosimetry (cellular scale	Realistic models showed clustering effects doubled absorbed dose vs geometric models; >50% cells received zero dose; stochastic modeling improved survival and RBE prediction	105
^{212}PbVMT01	Improvement of TAT cellular dosimetry accuracy by incorporating toxicity analysis, morphology changes and changes in biomarkers, focusing on the renal system	DiGiMouse voxel-based phantom models and OLINDA 2.1	^{212}PbVMT01 induced renal damage in the tubules in the kidney and not in the glomeruli. The escalation in doses resulted in doses between 0-24.6 Gy to the kidneys. A decrease in the number of red blood cells was observed at 30-week post-injection of 6.6Mbq.	106

Table 5 (*Continued*)

Macrodosimetry

Radiopharmaceutical	Objective	Dosimetry Methodology	Findings	Reference number
^{212}Pb-labeled peptides	Evaluate the absorbed dose of α- and β-emitting radioligands, with a focus on the effects when the peptide the isotope is labeled to, is altered	Monte Carlo Particle and Heavy ion transport code system (PHITS) and DiGi-Mouse voxel-based phantom models	^{212}Pb bound to different peptides deposited 20% more dose to the tumors, with the same renal dose deposition, thus reinforcing the idea of performing correct peptide labeling to ^{212}Pb to ensure good tumor control.	107

Nanodosimetry

Radiopharmaceutical	Objective	Dosimetry Methodology	Findings	Reference number
^{212}Pb	Evaluate the efficacy of α-, β-, and Auger electron-emitting radionuclides for targeted radionuclide therapy in early brain metastasis models	Monte Carlo simulation: Geant4-DNA	^{212}Pb showed higher DSB yields (7.64 $\pm$ 0.12 and 9.15 $\pm$ 0.24 per GbpGy compared to ^{177}Lu (2.69 $\pm$ 0.08 per GbpGy), suggesting better efficacy for short-range targeting of micrometastatic lesions.	108
^{212}Pb, ^{225}Ac, ^{223}Ra and ^{211}At	Evaluate the efficacy of double-stranded DNA breaks caused by α- particle transport and determine the absorbed dose to the nucleus when varying the binding location of the radionuclide	Monte Carlo simulation: Geant4, Geant4-DNA, TOPAS and TOPAS-nbio	^{212}Pb showed a higher percentage of alpha particles crossing the nucleus outer surface when the initial radionuclide location was in the cell membrane, as compared to ^{225}Ac, ^{223}Ra and ^{211}At. However, ^{225}Ac and ^{223}Ra exhibited a higher dose to the nucleus per decay as compared to ^{212}Pb and ^{211}At, thus suggesting that for effective therapy, cell surface binding is not sufficient, instead localized nuclear delivery near the nuclease will result in significant DNA damage	109
^{212}Pb and ^{212}Bi	Evaluate the dose contribution of β- and gamma particles and their non-localized energy deposition using a diffusion leakage model with dose point kernels	Monte Carlo simulation: TOPAS, COMSOL Multiphysics, DaRT	The absorbed dose contributions by beta and gamma particles were lower at radial distances $>$1.0 mm, as compared to ^{212}Bi, suggesting better localized dose delivery to the tumor and is desirable for organs at risk that surround the tumor volume.	110
^{212}Pb-anti-HER2/neu and ^{212}Pb-unlabelled	Evaluate the efficacy of the RBE of α-, β-, and Auger electron-emitting radionuclides for targeted radionuclide therapy using ^{212}Pb-anti/HER2/neu, as compared to unlabeled ^{212}Pb, for murine mammary carcinomas	Monte Carlo simulation: Geant4	^{212}Pb-anti/HER2/neu showed an RBE of 8.3 at 37% cell survival and a survival-independent RBE of 9.9 as compared to unlabeled ^{212}Pb. The unlabeled ^{212}Pb showed no significant absorbed dose induced cellular proliferation or clonogenic reduction, thus highlighting the importance of precise targeting for effective tumor cell killing	111

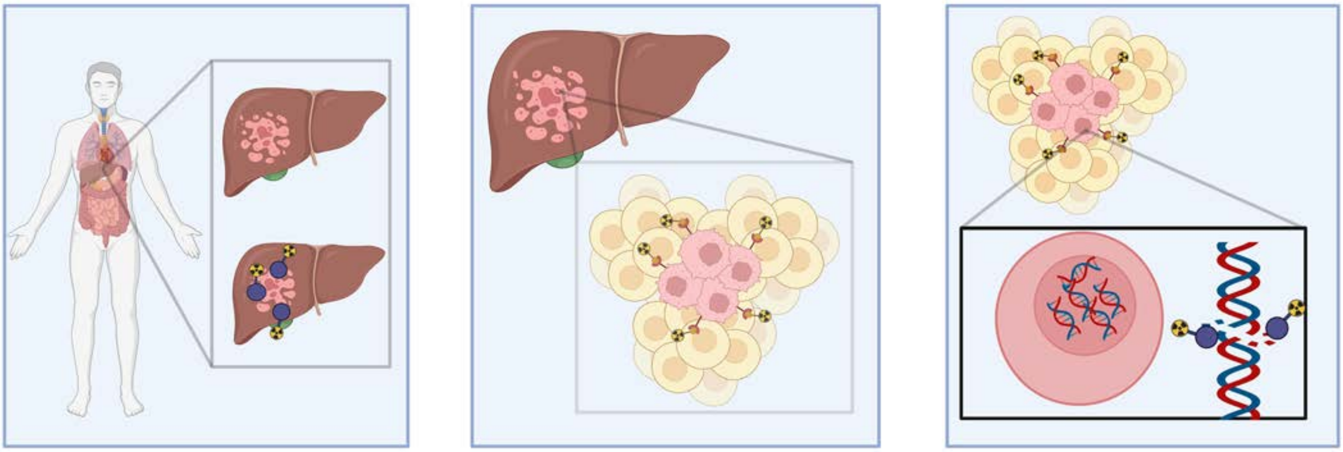

Figure 8 Multiscale Dosimetry of alpha Particles in ^{212}Pb-Targeted Alpha Therapy.(a) At the organ or tumor level, the short range of α-particles combined with heterogeneous uptake of ^{212}Pb-labeled vectors results in highly non-uniform absorbed dose distributions. (b) At the cellular scale, stochastic emission of α-particles and redistribution of short-lived daughters (^{212}Bi, ^{212}Po) cause substantial variability in dose deposition between adjacent cells. (c) At the subcellular level, α-particle tracks deliver densely ionizing radiation that induces clustered DNA lesions, driving the high relative biological effectiveness characteristic of ^{212}Pb-TAT.

stochastic nature of energy deposition at micrometer dimensions. In this framework, the specific energy (z) serves as the microdosimetric analogue of the absorbed dose.[101] It is defined as the ratio of the energy imparted by ionizing radiation (ε) to the mass of a small target volume (m). Unlike the absorbed dose, which represents a mean quantity, the specific energy is inherently stochastic, reflecting the probabilistic distribution of individual radiation interactions at microscopic scales.

Microdosimetry therefore, becomes essential to assess both therapeutic efficacy and normal tissue toxicity. At the cellular and subcellular scale, the localization of activity (eg, on the membrane, in the cytoplasm, or in the nucleus) critically determines the energy deposition in the nucleus and the probability of DNA damage. This makes ^{212}Pb particularly sensitive to assumptions about sub-cellular pharmacokinetics, as its alpha-emitting daughters (^{212}Bi, ^{212}Po) impart a highly localized dose.

Computational approaches for ^{212}Pb microdosimetry include analytical formalisms for simple geometries and full MC simulations (eg, Geant4-DNA, MCNPX, GATE) for realistic cell and tissue structures. These methods allow evaluation of self-dose and cross-dose within cell clusters, DVH in tumors, and stochastic distributions of specific energy at the micrometer scale. Such modelling has demonstrated that dose heterogeneity, rather than mean organ dose, is often the relevant predictor of both tumor control and toxicity in TAT.[96]

Incorporation of small-scale and microdosimetric models into the ^{203}Pb/^{212}Pb dosimetry framework enables bridges the gap between macroscopic TAC-derived residence times and the microscopic energy deposition patterns that determine therapeutic outcome in ^{212}Pb TAT. These findings are summarised in Table 5 and demonstrated in Figure 8.

The Emerging Impact of Artificial Intelligence on Targeted Alpha Therapy

Artificial intelligence (AI), particularly deep learning (DL), is increasingly applied to radiopharmaceutical therapy dosimetry, improving efficiency and accuracy in patient-specific workflows.[112,113] For ^{203}Pb/^{212}Pb theranostics, AI facilitates automated organ and tumor segmentation, reducing operator variability and expediting dose calculation.[114] DL models can enhance image quality through denoising, super-resolution reconstruction, and image synthesis from early acquired PET or surrogate images, enabling quantitative imaging with reduced patient burden.

Crucially, AI can generate voxel-wise dose maps from pretherapy surrogate imaging (^{203}Pb) to predict therapeutic (^{212}Pb) distributions, addressing intra-organ heterogeneity and non-uniform radiation dose deposition, which are common challenges in TAT.[115] Generative and CNN-based models have demonstrated improved dose prediction and organ segmentation accuracy while maintaining clinically acceptable error.[116]

Despite these advances, limitations include scarcity of comprehensive multi-institutional training datasets, variability in imaging protocols, and the need to account for daughter radionuclide redistribution in alpha-emitter decay chains. Standardization, rigorous validation, and integration of physiologically based pharmacokinetic modeling with AI will be essential to fully realize robust, patient-friendly dosimetry in ^{203}Pb/^{212}Pb theranostics.

Conclusion

The emerging theragnostic pair ^{203}Pb/^{212}Pb represents a powerful platform for quantitative imaging and personalized TAT. While ^{203}Pb enables accurate pre-therapeutic dosimetry through high-quality SPECT/CT imaging and robust pharmacokinetic modelling, translation to ^{212}Pb requires careful consideration of daughter nuclide migration, chelator stability, and the short-ranged, high-LET nature of emitted α-particles. Advances in image reconstruction, TAC fitting, and TIA estimation, combined with voxel-level and microdosimetric approaches, are refining the accuracy of absorbed dose calculations. Ultimately, integration of these methods into patient-specific dose computations provides the foundation for individualized treatment planning. Continued development of quantitative imaging, coupled with microdosimetric modelling, is expected to transform ^{212}Pb dosimetry from a conceptual framework into a clinically applicable tool, enabling safer, more effective, and personalized α-particle therapy.

Declaration of competing interest

The authors declare that they have no known competing financial interests or personal relationships that could have appeared to influence the work reported in this paper.

CRediT authorship contribution statement

Keamogetswe Ramonaheng: Conceptualization, Validation, Writing – original draft, Writing – review & editing. **Milani Qebetu:** Writing – review & editing. **Kaluzi Banda:** Software, Writing – review & editing. **Pryaska Goorhoo:** Writing – review & editing. **Khomotso Legodi:** Writing – review & editing. **Sipho Mdanda:** Writing – review & editing. **Sandile Sibiya:** Writing – review & editing. **Yonwaba Mzizi:** Writing – review & editing. **Honest Ndlovu:** Writing – review & editing. **Joseph Kabunda:** Writing – review & editing. **Mengdie Yang:** Writing – review & editing. **Kuangyu Shi:** Writing – review & editing. **Mike Sathekge:** Conceptualization, Validation, Writing – review & editing.

References

1. Lepareur N, Ramée B, Mougin-Degraef M, et al: Clinical advances and perspectives in targeted radionuclide therapy. Pharmaceutics 15 (6):1733, 2023
2. Ferro-Flores G, Azorín-Vega E, Ocampo-García B, et al: Effects of targeted radionuclide therapy on cancer cells beyond the ablative radiation dose. Int J Molecul Sci 26(14):6968, 2025
3. Bartlett M: From the inside out: Radionuclide radiation therapy. Australas Phys Eng Sci Med 39(2):357-359, 2016
4. Hardiansyah D, Guo W, Kletting P, et al: Time-integrated activity coefficient estimation for radionuclide therapy using PET and a pharmacokinetic model: A simulation study on the effect of sampling schedule and noise. Medical Physics 43(9):5145-5154, 2016
5. Iagaru AH, Mittra E, Colletti PM, et al: Bone-targeted imaging and radionuclide therapy in prostate cancer. J Nuclear Med 57(Supplement 3):19S-24S, 2016
6. Jin ZH, Furukawa T, Degardin M, et al: αVβ3 Integrin-targeted radionuclide therapy with 64Cu-cyclam-RAFT-c(-RGDfK-)4. Mol Cancer Ther 15(9):2076-2085, 2016
7. Kratochwil C, Bruchertseifer F, Rathke H, et al: Targeted α-therapy of metastatic castration-resistant prostate cancer with 225Ac-PSMA-617: Dosimetry estimate and empiric dose finding. J Nucl Med 58 (10):1624-1631, 2017
8. Kwekkeboom DJ, Krenning EP: Peptide receptor radionuclide therapy in the treatment of neuroendocrine tumors. Hematol/Oncol Clin North Am 30(1):179-191, 2016
9. Nonnekens J, van Kranenburg M, Beerens CEMT, et al: Potentiation of peptide receptor radionuclide therapy by the PARP inhibitor Olaparib. Theranostics 6(11):1821-1832, 2016
10. Norain A, Dadachova E: Targeted radionuclide therapy of melanoma. Sem Nuclear Med 46(3):250-259, 2016
11. Weber WA, Morris MJ: Molecular imaging and targeted radionuclide therapy of prostate cancer. J Nuclear Med 57(Supplement 3):3S-5S, 2016
12. Werner RA, Lapa C, Ilhan H, et al: Survival prediction in patients undergoing radionuclide therapy based on intratumoral somatostatin-receptor heterogeneity. Oncotarget 8(4):7039-7049, 2016
13. Zukotynski K, Jadvar H, Capala J, et al: Targeted radionuclide therapy: Practical applications and future prospects. Biomark Cancer 8(Suppl 2):35-38, 2016
14. Dekempeneer Y, Keyaerts M, Krasniqi A, et al: Targeted alpha therapy using short-lived alpha-particles and the promise of nanobodies as targeting vehicle. Exp Opinion Biol Ther 16(8):1035-1047, 2016
15. Makvandi M, Dupis E, Engle JW, et al: Alpha-emitters and targeted Alpha therapy in oncology: From basic science to clinical investigations. Targ Oncol 13(2):189-203, 2018
16. Sollini M, Marzo K, Chiti A, et al: The five “W”s and “how” of targeted alpha therapy: Why? Who? What? Where? When? And how? Rend Fis Acc Lincei 31(2):231-247, 2020
17. Kratochwil C, Bruchertseifer F, Giesel FL, et al: 225Ac-PSMA-617 for PSMA-targeted α-radiation therapy of metastatic castration-resistant prostate cancer. J Nucl Med 57(12):1941-1944, 2016
18. De Kruijff RM, Wolterbeek HT, Denkova AG: A critical review of alpha radionuclide therapy—How to deal with recoiling daughters? Pharmaceuticals 8(2):321-336, 2015
19. Marcu L, Bezak E, Allen BJ: Global comparison of targeted alpha vs targeted beta therapy for cancer: In vitro, in vivo and clinical trials. Crit Rev Oncol/Hematol. 123:7-20, 2018
20. Obata H, Ogawa M, Zalutsky MR: DNA repair inhibitors: Potential targets and partners for targeted radionuclide therapy. Pharmaceutics 15 (7):1926, 2023
21. Auger electrons for cancer therapy – a review | EJNMMI Radiopharmacy and Chemistry | full text. [Accessed August 21, 2025]. Available at: https://ejnmmipharmchem.springeropen.com/articles/10.1186/s41181-019-0075-2
22. Elgqvist J, Frost S, Pouget JP, et al: The potential and hurdles of targeted alpha therapy – Clinical trials and beyond. Front Oncol 3:324, 2014
23. Gape PMD, Schultz MK, Stasiuk GJ, et al: Towards effective targeted alpha therapy for neuroendocrine tumours: A review. Pharmaceuticals 17(3):334, 2024
24. Mavragani IV, Nikitaki Z, Kalospyros SA, et al: Ionizing radiation and complex DNA damage: From prediction to detection challenges and biological significance. Cancers 11(11):1789, 2019
25. Targeted alpha therapy: A comprehensive analysis of the biological effects from “local-regional-systemic” dimensions, Eur J Nuclear Med

Molecul Imag. [Accessed August 21, 2025]. Available from: https://link.springer.com/article/10.1007/s00259-025-07390-0

26. Coll RP, Bright SJ, Martinus DKJ, et al: Alpha particle—Emitting radiopharmaceuticals as cancer therapy: Biological basis, current status, and future outlook for therapeutics discovery. Mol Imaging Biol 25 (6):991-1019, 2023
27. Rumiantcev M, Li WB, Lindner S, et al: Estimation of relative biological effectiveness of 225Ac compared to 177Lu during [225Ac]Ac-PSMA and [177Lu]Lu-PSMA radiopharmaceutical therapy using TOPAS/TOPAS-nBio/MEDRAS. EJNMMI Phys 10(1):53, 2023
28. Sgouros G: Alpha-particles for targeted therapy. Adv Drug Delivery Rev 60(12):1402-1406, 2008
29. Sgouros G, Roeske JC, McDevitt MR, et al: MIRD pamphlet No. 22 (Abridged): Radiobiology and dosimetry of α-particle emitters for targeted radionuclide therapy. J Nuclear Med 51(2):311-328, 2010
30. Li WB, Hofmann W, Friedland W: Microdosimetry and nanodosimetry for internal emitters. Radiat Measurem 115:29-42, 2018
31. Behr TM, Béhé M, Stabin MG, et al: High-linear energy transfer (LET) alpha versus low-LET beta emitters in radioimmunotherapy of solid tumors: Therapeutic efficacy and dose-limiting toxicity of 213Bi- versus 90Y-labeled CO17-1A Fab' fragments in a human colonic cancer model. Cancer Res 59(11):2635-2643, 1999
32. Hauck ML, Larsen RH, Welsh PC, et al: Cytotoxicity of alpha-particle-emitting astatine-211-labelled antibody in tumour spheroids: No effect of hyperthermia. Br J Cancer 77(5):753-759, 1998
33. Jurcic JG, Larson SM, Sgouros G, et al: Targeted alpha particle immunotherapy for myeloid leukemia. Blood 100(4):1233-1239, 2002
34. Kim YS, Brechbiel MW: An overview of targeted alpha therapy. Tumour Biol 33(3):573-590, 2012
35. Macklis RM, Kinsey BM, Kassis AI, et al: Radioimmunotherapy with alpha-particle-emitting immunoconjugates. Science 240(4855):1024-1026, 1988
36. Sgouros G, Song H: Cancer stem cell targeting using the alpha-particle emitter, 213Bi: Mathematical modeling and feasibility analysis. Cancer Biother Radiopharm 23(1):74-81, 2008
37. Zalutsky MR: Targeted alpha-particle therapy of microscopic disease: Providing a further rationale for clinical investigation. J Nucl Med 47 (8):1238-1240, 2006
38. Tranel J, Feng FY, James SS, et al: Effect of microdistribution of alpha and beta-emitters in targeted radionuclide therapies on delivered absorbed dose in a GATE model of bone marrow. Phys Med Biol 66 (3):035016, 2021
39. Zhang J, Qin S, Yang M, et al: Alpha-emitters and targeted alpha therapy in cancer treatment. iRADIOLOGY 1(3):245-261, 2023
40. Kozempel J, Mokhodoeva O, Vlk M: Progress in targeted alpha-particle therapy. What we learned about recoils release from In vivo generators. Molecules 23(3):581, 2018
41. Trujillo-Nolasco M, Morales-Avila E, Cruz-Nova P, et al: Nanoradiopharmaceuticals based on alpha emitters: Recent developments for medical applications. Pharmaceutics 13(8):1123, 2021
42. Ree SM, Greenwood H, Young JD, et al: Selection of radionuclide(s) for targeted alpha therapy based on their nuclear decay properties. Nucl Med Commun 45(6):465-473, 2024
43. Nelson BJB, Andersson JD, Wuest F: Targeted alpha therapy: Progress in radionuclide production, radiochemistry, and applications. Pharmaceutics 13(1):49, 2020
44. Meredith R, Torgue J, Shen S, et al: Dose escalation and dosimetry of first-in-Human α radioimmunotherapy with 212Pb-TCMC-Trastuzumab. J Nuclear Med 55(10):1636-1642, 2014
45. Meredith RF, Torgue J, Azure MT, et al: Pharmacokinetics and imaging of 212Pb-TCMC-Trastuzumab after intraperitoneal administration in ovarian cancer patients. Cancer Biother Radiopharmaceut 29(1):12-17, 2014
46. Eckerman K, Endo A: ICRP Publication 107. Nuclear decay data for dosimetric calculations. Ann ICRP 38(3):7-96, 2008
47. Kvassheim M, Revheim MER, Stokke C: Quantitative SPECT/CT imaging of lead-212: A phantom study. EJNMMI Phys 9:52, 2022
48. McNeil BL, Mastroianni SA, McNeil SW, et al: Optimized production, purification, and radiolabeling of the 203Pb/212Pb theranostic pair for nuclear medicine. Sci Rep 13(1):10623, 2023
49. Martin MJ: Nuclear data sheets for A = 208. Nuclear Data Sheets 108 (8):1583-1806, 2007
50. Griffiths MR, Pattison DA, Latter M, et al: First-in-Human 212Pb-PSMA—Targeted α-therapy SPECT/CT imaging in a patient with metastatic castration-resistant prostate cancer. J Nuclear Med 2024. [Accessed May 29, 2024]Available at: https://jnm.snmjournals.org/content/early/2024/02/29/jnumed.123.267189
51. Saini S, Bartels JL, Appiah JPK, et al: Optimized methods for the production of high-purity 203Pb using electroplated thallium targets. J Nucl Med 64(11):1791-1797, 2023
52. Nelson BJB, Wilson J, Schultz MK, et al: High-yield cyclotron production of 203Pb using a sealed 205Tl solid target. Nucl Med Biol 116-117:108314, 2023
53. Miao Y, Figueroa SD, Fisher DR, et al: 203Pb-labeled alpha-melanocyte-stimulating hormone peptide as an imaging probe for melanoma detection. J Nucl Med 49(5):823-829, 2008
54. Baidoo KE, Milenic DE, Brechbiel MW: Methodology for labeling proteins and peptides with lead-212 (212Pb). Nucl Med Biol 40(5):592-599, 2013
55. Stenberg VY, Juzeniene A, Bruland ØS, et al: In situ generated 212Pb-PSMA Ligand in a 224Ra-solution for dual targeting of prostate cancer sclerotic stroma and PSMA-positive cells. Curr Radiopharm 13 (2):130-141, 2020
56. Hierlmeier I, Randhawa P, McNeil BL, et al: Radiochemistry of cyclen-derived chelators comprising five-membered azaheterocyclic arms with 212Pb2+, 213Bi3+, and 225Ac3+. Nuclear Med Biol 146—147:109034, 2025
57. Chapeau D, Koustoulidou S, Handula M, et al: 212Pb]Pb-eSOMA-01: A promising radioligand for targeted alpha therapy of neuroendocrine tumors. Pharmaceutics 16(7):985, 2023
58. Li M, Baumhover NJ, Liu D, et al: Preclinical evaluation of a lead specific chelator (PSC) conjugated to radiopeptides for 203Pb and 212Pb-based theranostics. Pharmaceutics 15(2):414, 2023
59. Kokov KV, Egorova BV, German MN, et al: 212Pb: Production approaches and targeted therapy applications. Pharmaceutics 14 (1):189, 2022
60. Delpassand ES, Tworowska I, Esfandiari R, et al: Targeted α-emitter therapy with 212Pb-DOTAMTATE for the treatment of metastatic SSTR-expressing neuroendocrine tumors: First-in-humans dose-escalation clinical trial. J Nucl Med 63(9):1326-1333, 2022
61. Stumpp MT, Binz HK, Amstutz P: DARPins: A new generation of protein therapeutics. Drug Discov Today 13(15—16):695-701, 2008
62. dos Santos JC, Schäfer M, Bauder-Wüst U, et al: Development and dosimetry of ^{203}Pb/^{212}Pb-labelled PSMA ligands: Bringing "the lead" into PSMA-targeted alpha therapy? Eur J Nucl Med Mol Imaging 46 (5):1081-1091, 2019
63. Miao Y, Hylarides M, Fisher DR, et al: Melanoma therapy via peptide-targeted α-radiation. Clin Cancer Res 11(15):5616-5621, 2005
64. Yong K, Brechbiel M: Application of 212Pb for targeted α-particle therapy (TAT): Pre-clinical and mechanistic understanding through to clinical translation. AIMS Med Sci 2(3):228-245, 2015
65. Juzeniene A, Stenberg VY, Bruland ØS, et al: Dual targeting with ^{224}Ra/^{212}Pb-conjugates for targeted alpha therapy of disseminated cancers: A conceptual approach. Front Med. 9, 2023. [Accessed August 28, 2025]Available at: https://www.frontiersin.org/journals/medicine/articles/10.3389/fmed.2022.1051825/full
66. Lin FI, Del RJ, Thomas A, et al: Phase 1 trial of Pb-212-VMT-alpha-NET in select metastatic or inoperable somatostatin receptor positive tumors. Endocrine Abstracts 98, 2023. [Accessed August 21, 2025]Available at: https://www.endocrine-abstracts.org/ea/0098/ea0098t7
67. Sen I, Malik D, Thakral P, et al: 212Pb-VMT-Î±-NET targeted alpha therapy in metastatic neuroendocrine tumors: First in Human study on safety and efficacy. J Nuclear Med 65(supplement 2), 2024. 242556-242556
68. medical.orano.group. 99AD [Accessed August 21, 2025]. Orano Med starts phase I trial with Alpha radioligand therapy 212Pb-GRPR in patients with solid tumors. Available at: https://www.oranomed.com/en/resources/news/2023/orano-med-starts-phase-1-trial-with-alpha-radioligand-therapy-212pb-grpr-in-patients-with-solid-tumors

69. Molecular Partners outlines clinical expansion plans and strengthens Radiopharma strategic focus for 2025 at 43rd Annual J.P. Morgan Healthcare Conference, Molecul Part. [Accessed August 21, 2025]. Available at: https://investors.molecularpartners.com/news-releases/news-release-details/molecular-partners-outlines-clinical-expansion-plans-and/
70. Massari R, Mok GSP: Editorial: New trends in single photon emission computed tomography (SPECT). Front Med 10, 2023. [Accessed August 28, 2025]Available at: https://www.frontiersin.org/journals/medicine/articles/10.3389/fmed.2023.1349877/full
71. Fani M, Maecke HR: Radiopharmaceutical development of radiolabelled peptides. Eur J Nucl Med Mol Imaging 39(1):11-30, 2012
72. Martin ME, Sue O'Dorisio M, Leverich WM, et al: Click"-cyclized 68Ga-labeled peptides for molecular imaging and therapy: Synthesis and preliminary In vitro and In vivo evaluation in a melanoma model system. In: Baum RP, Rösch F (eds): Theranostics, gallium-68, and other radionuclides, Berlin, Heidelberg: Springer, 149-175, 2013
73. Koulikov V, Lerman H, Kesler M, et al: 99mTc-MDP bone scintigraphy of the hand: Comparing the use of novel cadmium zinc telluride (CZT) and routine NaI(Tl) detectors. EJNMMI Res 5:63, 2015
74. Melodia L. Deep learning estimation of absorbed dose for nuclear medicine diagnostics. arXiv; 2022 [Accessed September 1, 2025]. Available at: http://arxiv.org/abs/1805.09108
75. Willowson KP, Bailey DL: Evolving SPECT-CT technology. Br J Radiol: tqae200, 2024.
76. Zorz A, Rossato MA, Turco P, et al: Performance evaluation of the 3D-ring cadmium-zinc-telluride (CZT) StarGuide system according to the NEMA NU 1-2018 standard. EJNMMI Phys 11(1):69, 2024
77. Kästner D, Hartmann H, Freudenberg R, et al: Gamma camera imaging characteristics of $^{203/212}$Pb as a theragnostic pair for targeted alpha therapy: A feasibility study. EJNMMI Phys 12(1):50, 2025
78. Cosmi V, Wang B, Goorden MC, et al: NaI gamma camera performance for high energies: Effects of crystal thickness, photomultiplier tube geometry and light guide thickness. Med Phys 51(7):4696-4708, 2024
79. Madsen MT: Recent advances in SPECT imaging. J Nucl Med 48 (4):661-673, 2007
80. Oddstig J, Hedeer F, Jögi J, et al: Reduced administered activity, reduced acquisition time, and preserved image quality for the new CZT camera. J Nuclear Cardiol 20(1):38-44, 2013
81. Duvall WL, Croft LB, Ginsberg ES, et al: Reduced isotope dose and imaging time with a high-efficiency CZT SPECT camera. J Nuclear Cardiol 18(5):847-857, 2011
82. Menda Y, Madsen MT, O'Dorisio TM, et al: ^{90}Y-DOTATOC dosimetry-based personalized peptide receptor radionuclide therapy. J Nucl Med 59(11):1692-1698, 2018
83. Ramonaheng K, Qebetu M, Ndlovu H, et al: Activity quantification and dosimetry in radiopharmaceutical therapy with reference to ^{177}Lutetium. Front Nucl Med 4, 2024. [Accessed May 23, 2024]Available at: https://www.frontiersin.org/articles/10.3389/fnume.2024.1355912
84. Tronchin S, Forster JC, Hickson K, et al: Dosimetry in targeted alpha therapy. A systematic review: Current findings and what is needed. Phys Med Biol 67(9):09TR01, 2022
85. AnyScan - Mediso - PDF catalogs, Technical documentation. [Accessed September 1, 2025]. Available at: https://pdf.medicalexpo.com/pdf/mediso/anyscan/94149-115577.html
86. Michler E, Kästner D, Brogsitter C, et al: First-in-human SPECT/CT imaging of [^{212}Pb]Pb-VMT-α-NET in a patient with metastatic neuroendocrine tumor. Eur J Nucl Med Mol Imaging 51(5):1490-1492, 2024
87. Graves S, Li M, Lee D, et al: On the use of ^{203}Pb imaging to inform ^{212}Pb dosimetry for $^{203/212}$Pb image-guided alpha-particle therapy for cancer. In: Prasad V (ed): Beyond Becquerel and Biology to Precision Radiomolecular Oncology: Festschrift in Honor of Richard P Baum, Cham: Springer International Publishing, 277-287. https://doi.org/10.1007/978-3-031-33533-4_28, 2024
88. Graves S, Bushnell D, Schultz M, et al: 212Pb-VMT-Î±-NET Î±-PRRT planning based on ^{203}Pb-VMT-Î±-NET predictive dosimetry. J Nuclear Med 65(supplement 2), 2024. 242110-242110
89. Kvassheim M, Tornes AJK, Juzeniene A, et al: Imaging of ^{212}Pb in mice with a clinical SPECT/CT. EJNMMI Phys 10(1):47, 2023
90. Banerjee SR, Minn I, Kumar V, et al: Preclinical evaluation of $^{203/212}$Pb-labeled low-molecular-weight compounds for targeted radiopharmaceutical therapy of prostate cancer. J Nucl Med 61(1):80-88, 2020
91. Desy A, Bouvet GF, Croteau É, et al: Quantitative SPECT (QSPECT) at high count rates with contemporary SPECT/CT systems. EJNMMI Phys 8(1):73, 2021
92. Michler E, Kästner D, Pretze M, et al: $^{203/212}$Pb]Pb-VMT-α-NET as a novel theranostic agent for targeted alpha radiotherapy—First clinical experience. Eur J Nucl Med Mol Imaging 2025. https://doi.org/10.1007/s00259-025-07269-0. [Accessed June 21, 2025]
93. Jain S, Graves S, Bodeker K, et al: Optimal imaging timepoint for diagnostic performance of ^{203}Pb-VMT-Î±-NET SPECT/CT in neuroendocrine tumors. J Nuclear Med 65(supplement 2), 2024. 242347-242347
94. Müller D, Herrmann H, Schultz MK, et al: 203 Pb-VMT-α-NET scintigraphy of a patient with neuroendocrine tumor. Clin Nucl Med 48 (1):54-55, 2023
95. He B, Frey E, Sgouros G, et al: Development and validation of methods for quantitative In vivo SPECT of Pb-212. J Med Imag Radiat Sciences 50(1):S33, 2019
96. Danieli R, Milano A, Gallo S, et al: Personalized dosimetry in targeted radiation therapy: A look to methods, tools and critical aspects. J Personalized Med 12(2):205, 2022
97. Hindorf C, Glatting G, Chiesa C, et al: EANM Dosimetry Committee guidelines for bone marrow and whole-body dosimetry. Eur J Nucl Med Mol Imag 37(6):1238-1250, 2010
98. Mirzadeh S, Kumar K, Gansow OA: The chemical fate of 212Bi-DOTA formed by β decay of 212Pb(DOTA)2-. Radiochimica Acta 60(1):1-10, 1993
99. Gansow OA, Wu C: Advanced methods for radiolabeling monoclonal antibodies with therapeutic radionuclides. In: Cancer therapy with radiolabeled antibodies. First Edition. CRC Press: Boca Raton, 1995
100. Bolch WE, Eckerman KF, Sgouros G, et al: MIRD pamphlet No. 21: A generalized schema for radiopharmaceutical dosimetry—Standardization of nomenclature. Journal of Nuclear Medicine 50(3):477-484, 2009
101. ICRU Report 83, prescribing, recording, and reporting intensity-modulated photon-beam therapy (IMRT), ICRU. [Accessed August 31, 2025]. Available at: https://www.icru.org/report/prescribing-recording-and-reporting-intensity-modulated-photon-beam-therapy-imrticru-report-83/
102. Li M, Robles-Planells C, Liu D, et al. Pre-clinical evaluation of biomarkers for early detection of nephrotoxicity following alpha-particle radioligand therapy. bioRxiv. 2023;2023.09.27.559789.
103. Orcutt KD, Henry KE, Habjan C, et al: Dosimetry of [212Pb]VMT01, a MC1R-targeted alpha therapeutic compound, and effect of free 208Tl on tissue absorbed doses. Molecules 27(18):5831, 2022
104. Fongenie B, Scott N, Chouin N, et al: Dosimetry-driven alpha emitter selection for Radioligand therapy: A real world application comparing 225Ac with 212Pb. medRxiv 2025:25333110. [Accessed August 21, 2025]. Available at: https://www.medrxiv.org/content/10.1101/2025.08.08.25333110v1
105. Bastiaannet R, Liatsou I, Hobbs R F, Sgouros G: Large-scale in vitro microdosimetry via live cell microscopy imaging: Implications for radiosensitivity and RBE evaluations in alpha-emitter radiopharmaceutical therapy. J Translat Med 21(1):144, 2023
106. Li M, Sagastume E, Zepeda-Orozco D, et al: Preclinical evaluation of 203/212Pb-based theranostics-dosimetry and renal toxicity. J Nuclear Med 61(supplement 1), 2020. 289-289
107. Lee D, Li M, Liu D, et al: Structural modifications toward improved lead-203/lead-212 peptide-based image-guided alpha-particle radiopharmaceutical therapies for neuroendocrine tumors. Eur J Nucl Med Mol Imaging 51(4):1147-1162, 2024
108. Falzone N, Ackerman NL, Rosales L, et al: Dosimetric evaluation of radionuclides for VCAM-1-targeted radionuclide therapy of early brain metastases. Theranostics 8(1):292-303, 2018
109. Penfold SN, Brown MP, Staudacher AH, et al: Monte Carlo simulations of dose distributions with necrotic tumor targeted radioimmunotherapy. Appl Radiat Isot 90:40-45, 2014

110. Khan AU, Jollota S, DeWerd LA: A diffusion-leakage model coupled with dose point kernels (DPK) for dosimetry of diffusing alpha-emitters radiation therapy (DaRT). Med Phys 51(5):3725-3733, 2024
111. Liatsou I, Yu J, Bastiaannet R, et al: 212Pb-conjugated anti-rat HER2/neu antibody against a neu-N derived murine mammary carcinoma cell line: Cell kill and RBE in vitro. Int J Radiat Biol 98(9):1452-1461, 2022
112. Yazdani E, Geramifar P, Karamzade-Ziarati N, et al: Radiomics and Artificial intelligence in radiotheranostics: A review of applications for radioligands targeting somatostatin receptors and prostate-specific membrane antigens. Diagnostics 14(2):181, 2024
113. Mansouri Z, Salimi Y, Akhavanallaf A, et al: Deep transformer-based personalized dosimetry from SPECT/CT images: A hybrid approach for [177Lu]Lu-DOTATATE radiopharmaceutical therapy. Eur J Nucl Med Mol Imag 51(6):1516-1529, 2024
114. Brosch-Lenz J, Yousefirizi F, Zukotynski K, et al: Role of artificial intelligence in theranostics:: Toward routine personalized radiopharmaceutical therapies. PET Clin 16(4):627-641, 2021
115. Xue S, Gafita A, Zhao Y, et al: Pre-therapy PET-based voxel-wise dosimetry prediction by characterizing intra-organ heterogeneity in PSMA-directed radiopharmaceutical theranostics. Eur J Nucl Med Mol Imag 51(11):3450-3460, 2024
116. Liu J, Zhang X, Cheng X, et al: A deep learning-based dose prediction method for evaluation of radiotherapy treatment planning. J Radiat Res Appl Sci 17(1):100757, 2024